INTERNATIONAL ATOMIC ENERGY AGENCY
UNITED NATIONS EDUCATIONAL, SCIENTIFIC AND CULTURAL ORGANIZATION
INTERNATIONAL CENTRE FOR THEORETICAL PHYSICS
I.C.T.P., P.O. BOX 586, 34100 TRIESTE, ITALY, CABLE: CENTRATOM TRIESTE

UNITED NATIONS INDUSTRIAL DEVELOPMENT ORGANIZATION

INTERNATIONAL CENTRE FOR SCIENCE AND HIGH TECHNOLOGY
c/o INTERNATIONAL CENTRE FOR THEORETICAL PHYSICS 34100 TRIESTE (ITALY) VIA GRIGNANO, 9 (ADRIATICO PALACE) P.O. BOX 586 TELEPHONE 040-224572 TELEFAX 040-224575 TELEX 460449 APH I

SMR/760-20

"College on Atmospheric Boundary Layer and Air Pollution Modelling"
16 May - 3 June 1994

"Observing and Modelling the Planetary Boundary Layer"

Presented by: S. ZILITINEVICH
Alfred-Wagner-Institut für Polar
und Meeresforschung
Bremerhaven, Germany

Please note: These notes are intended for internal distribution only.

Chapter 14

OBSERVING AND MODELLING THE PLANETARY BOUNDARY LAYER

Søren E. Larsen
Department of Meteorology and Wind Energy
Risø National Laboratory
Denmark

14.1 Introduction

Characteristics of the atmospheric planetary boundary layer (PBL) are important for the atmospheric energy and water cycles because the fluxes of momentum, heat, and water vapour between the atmosphere and the surfaces of the earth all pass through the PBL, being carried and modified by mixing processes here. Since these mixing processes mostly owe their efficiency to the mechanisms of boundary layer turbulence, a proper quantitative description of the turbulence processes becomes essential for a satisfying description of the fluxes between the surface and the atmosphere.

Estimating the water and energy fluxes through the atmospheric boundary layers necessitates that almost all types of the flows, that occur there, must be considered. There are very few combinations of characteristic boundary layer conditions that are not of significant importance for the flux of energy and water between the surface and the atmosphere, at least for some parts of the globe.

14.2 Simple pictures and some basic statistical tools

Fluxes across the planetary boundary layer, PBL, are dominated by turbulent motion. Many pages have been filled in an effort to define turbulence. Here we shall just notice that motions of systems, that can be described by the nonlinear fluid equations, tend to show strongly varying stochastic components, the turbulence, as well as more smooth and predictable characteristics. In the PBL the wind speed as well as temperature and humidity show this stochastic behavior on all spatial and

NATO ASI Series, Vol. I 5
Energy and Water Cycles in the Climate System
Edited by E. Raschke and D. Jacob

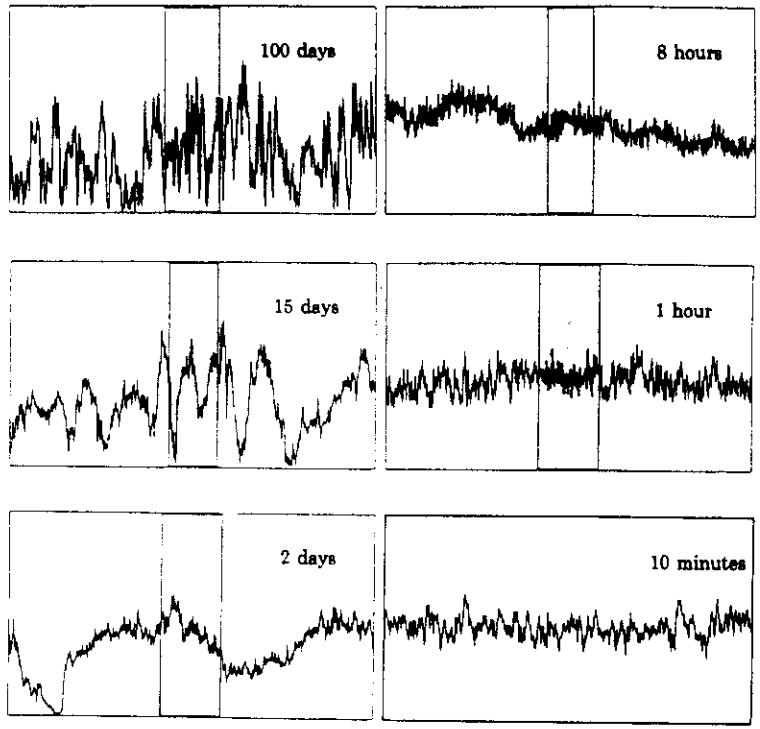

Figure 14.1: *Wind speed measured 30 m above flat homogeneous terrain in Denmark from Troen and Petersen (1989). The data were obtained from a one-year time series recorded with 16-Hz resolution. Each graph shows the measured wind speed over the time period indicated. The number of data points in each graph is 1200, each averaged over 1/1200 of the time period indicated. The vertical axis is wind speed, 0-20 ms^{-1}.*

temporal scales of variation. In Figure 14.1 this is illustrated by a measured time series of the wind speed observed through different time windows.

We shall mostly consider fluctuations on time scales of the order of and less than one hour, because the turbulence processes here carry most of the vertical fluxes, we will try to estimate.

On these time scales the main mechanism for producing turbulence is the vertical gradient of the mean wind. In Figure 14.2 we show typical vertical variations of wind speed, humidity, and temperature between their surface values and values at the top and above the PBL. Temperature and humidity can both increase and decrease with height depending on whether their surface values or values in the free atmosphere are the larger. However, the wind speed will always increase with height from zero at the ground to its value in the free atmosphere just above the PBL. This vertical wind shear gives rise to overturning of the air, producing the turbulence (Tennekes and Lumley,1982). This provides a formidable mechanism for carrying the vertical fluxes compared to the molecular transport mechanism that would have been an alternative. For example, a temperature gradient of

2 K between the surface and 10 meter height with a wind speed at 5 ms^{-1} gives rise to a heat flux of about 0.5 mKs^{-1} If for the same situation the flux had to be carried by molecular diffusion only, the result would be 4×10^{-6} mKs^{-1} only.

The temperature structure of the PBL strongly influences the turbulence production through its influence on the density of the air. If the air is warmer and thereby lighter close to the ground, it will enhance the production; if it is cooler at the ground the production will be reduced. To a lesser extent the humidity has similar, although smaller effects because also admixture of the water vapour changes the density of the air.

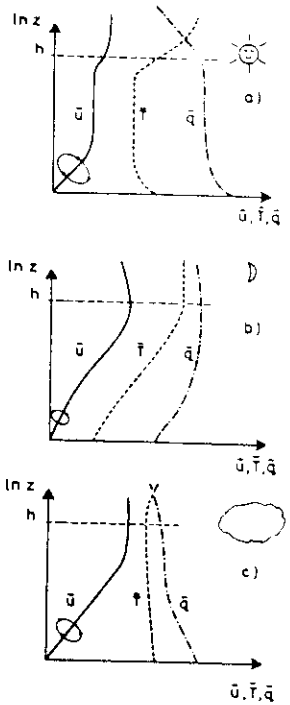

Figure 14.2: *Characteristic height variation (profiles) of the mean values of the wind speed, $\bar{u}$, temperature, $\bar{T}$, and humidity , $\bar{q}$ from the ground to the top of the PBL, indicated by h. Also shown by the arrows on the u-profile is the overturning of the flow induced by the vertical velocity gradient. The profiles are shown for the following characteristic situations: (a) thermally unstable, e.g. a sunny day, (b) thermally stable, e.g. a clear sky night, and, (c) thermally neutral, e.g. a high-wind overcast situation.*

Based on the above discussion we can now specify the planetary boundary layer as being the layer through which the atmospheric variables change between their values in the free atmosphere and their values at the surface, the transition being mostly controlled by turbulent motion and mixing.

In Figure 14.2 the turbulence production is envisioned as a swirling motion induced by the shear. This whorl constitutes a volume of localized vorticity which we shall denote an *eddy*. This picture of turbulence, as a soup of intertwining spaghetti-like eddies, has been very useful in the study of turbulence in spite of its extreme simplicity. Each eddy can be associated with a size, or spatial scale, and a lifetime. When the eddies have been produced they will remain coherent for some time, creating their own smaller shear regions. By the same process as for the mean shear these both erode the larger eddies, due to the associated mixing, and create smaller eddies. This mechanism repeats itself transferring energy to smaller and smaller eddies until they become small enough for the molecular viscosity to dissipate their motion into heat.

In view of the above discussion we shall next consider a few of the statistical tools used to describe the turbulence.

As the simplest we break down the signal into its mean value and its fluctuating part, e.g. for the variable x

$$x = \bar{x} + x' \tag{14.1}$$

where we use an overbar to signify the mean value while the symbol $'$ indicates the fluctuating part. This expansion is called the Reynolds expansion. Note that it implies $\overline{x'} = 0$. The averaging processes used to obtain $\bar{x}$ depend on the type of signal available and the purpose of averaging. In statistics one often talks about ensemble average over an ensemble of realizations of the signal x. This is the type of averaging used for most theoretical manipulations. In practice one will often use time or space averages, either because the signals available are a function of these parameters as e.g for measurements of time series from meteorological towers, or because of the objectives of the study as for example to obtain the area averages often being the goal of hydrological studies. The averaging procedures employed are limited by the signals available but are also a matter of choice. As an example, we can take the signal in Figure 14.1 that would lend itself to time averaging, since it is a time signal, but also to ensemble averaging using ensembles of data from similar days or hours.

Typical height variation of mean quantities as $\bar{u}, \bar{q}$, and $\bar{T}$ is illustrated in Figure 14.2 and the associated discussion. To further study the behavior of x', the simplest measures applicable are:

$$\begin{aligned} \text{the variance} &= \overline{x'^2} \\ \text{the covariance} &= \overline{x'y'} \end{aligned} \tag{14.2}$$

where y is another signal similar to x.

The variance is used to describe the fluctuation intensity of x, while $\overline{x'y'}$ can be used to study the relation between the two signals. Having considered the variances and covariances one can consider higher-order moments, and the distribution functions of the signals to study different aspects of their behavior. However, since it will not be much used here, we shall proceed to the tools used to identify the scales of variation.

Here the Fourier transform is often used to reveal the relevant scales. To analyse a time series like the one used in Figure 14.1, it is convenient to use the following Fourier expansion:

$$x'(t) = \int_{-\infty}^{\infty} dZ_x(\omega)\exp(i\omega t) \tag{14.3}$$

where $x'(t)$ is assumed to be a statistically stationary function of time. The Fourier expansion applied in Eq. 14.3 is the Fourier-Stieltje expansion that can be used even when $x(t)$ cannot be Fourier expanded in the standard sense, since it is not integrable (Lumley and Panofsky, 1964). The Fourier modes are here denoted $dZ(\omega)$ and are stochastic functions as well, being a function of the frequency ω[rad./sec]. Squaring and averaging, one finds from Eq. 14.3 that

$$\overline{x'^2} = \int_{-\infty}^{\infty} S_x(\omega)d\omega \tag{14.4}$$

where $S_x(\omega)$ is denoted the power density spectrum, or shorter simply the power spectrum of the $x(t)$, and it is seen to describe the contribution from the different frequencies to the variance of $x(t)$. This illustrates how the Fourier transform can be used to identify the important scales of variation, in this case the frequency scales. We present in Figure 14.3 the power spectrum of the one-year wind speed record used in Figure 14.1. In Figure 14.3 the spectrum is plotted versus the logarithm of the frequency because of the many decades of frequency scales of interest in geophysical time series. To obtain a proper impression of the contributions of the different frequency decades to the total variance, the spectrum is multiplied by the frequency, $f[Hz]$ because

$$\omega S(\omega)d(\ln(\omega)) = fS(f)d(\ln(f)) = S(\omega)d\omega \tag{14.5}$$

The strong intensity of the spectrum between the annual and the diurnal frequencies comes from the motion of the weather systems across Denmark. Therefore, it is different in other parts of the earth with different climatology as are of course the intensities of the diurnal and annual cycles. The contribution from the boundary layer turbulence described above is represented by the small bump from about 1 hour and out. Around 1 hour is the famous gap between what in relation to the boundary layer turbulence can be considered as the *mean flow* and the turbulence. This is mainly produced by the vertical shear in the mean flow, as discussed above.

There have been some discussion about the existence of this gap. This is because some convection clouds actually create eddies with about the time scale of the gap, see Fig. 14.4, and also since the spectra so far used to illustrate its existence often have been composited from different time series used to compute different decades of the total spectrum. From the point of view of modelling it is advantageous to use grid sizes with frequency and spatial scales within the spectral gap, because the absence of intensity here shows that only few independent processes create variability in this scale region. This in turn means that it becomes simpler to decide if a particular process must be parameterized or resolved explicitely by the model.

As stated above the spatial variability is most important for the structure of the boundary layer turbulence. Therefore, we shall finish this section by considering the wave-number spectrum and the quite general insight that can be drawn from the form of this spectrum.

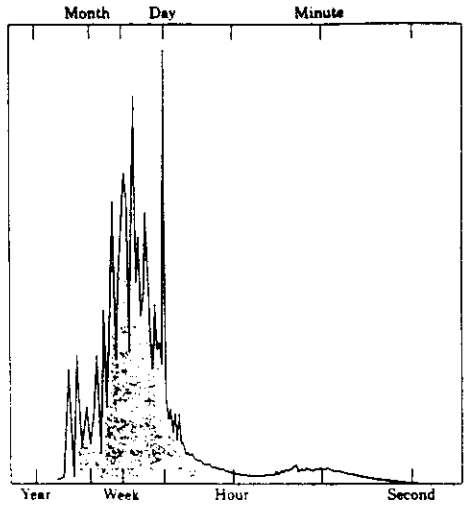

Figure 14.3 *The power spectrum of the one-year time series of wind speed versus the logarithm of the frequency, presented as the corresponding time periods (Courtney and Troen, 1990; Troen and Petersen, 1989).*

For a signal $x(t,\mathbf{r})$, being a stochastic statistically stationary and homogenous function of both time and the three spatial coordinates, $\mathbf{r}$, the spatial Fourier transform corresponding to Eq. 14.3 can be written:

$$x'(t,\mathbf{r}) = \int_{-\infty}^{\infty}\int_{-\infty}^{\infty}\int_{-\infty}^{\infty} dZ_x(t,k)\exp(i\mathbf{k}\cdot\mathbf{r}) \tag{14.6}$$

where $\mathbf{k}$ is now the wave-number vector. As previously we square the equation to obtain

$$\overline{x'^2} = \int_{-\infty}^{\infty}\int_{-\infty}^{\infty}\int_{-\infty}^{\infty} S_x(\mathbf{k})d\mathbf{k} \tag{14.7}$$

which shows how the variance distributes in the three-dimensional wave number space. Note that the time dependency disappears due to the stationarity assumption. For boundary-layer turbulence, strict use of Eq. 14.7 is not possible because even for the most homogeneous of all boundary layers there must be inhomogeneity in the vertical direction by the definition of a boundary layer. However, recall the picture of the eddies being created by mean shear and cascading the energy to smaller and smaller scales. We now assume that the spectral intensity at wave number k is an expression of the contribution to the total variance from eddies with linear size scale, $\ell \sim k^{-1}$. Furthermore, we assume that a range in k (or ℓ) exists where eddies have lost their memory about the orientation of the mean shear, being important only for the largest eddies, but still do not directly feel the effect of dissipation. For these scales the flow can be considered not only homogeneous in all directions, but

also isotropic. The latter means that the spectrum is only a function of the scalar wave number, k and the final dissipation of the variance of x. From this very simple idea one obtain the well known -5/3-law spectra (e.g. Tennekes and Lumley, 1982):

$$S_u(k) = a_u \epsilon^{2/3} k^{-5/3} \tag{14.8}$$

for velocity where ϵ symbolizes the dissipation of velocity fluctuations by molecular viscocity. For any of the scalars, x, like temperature, T, humidity, q and others, the expressions become

$$S_x(k) = a_x \epsilon^{-1/3} N_x k^{-5/3} \tag{14.9}$$

where N_x is the dissipation of scalar x, and the appearance of ϵ reflects the dominating importance of the velocity turbulence. The fluctuations of the scalars are considered to be the result of this carrying along as passive tracers by the air motion.

The spectral formulations in Eqs. 14.8 and 14.9 are called the inertial forms, and the empirical coefficients in front, a_u and a_x, the Kolmogorov constants for velocity and scalars, respectively. There are strong arguments and some empirical evidence that a_x is the same for all passive scalars (Hill, 1989).

When the spectral forms above apply, it is seen that the turbulence intensity for a given scale is characterised by its scale ($l \sim k^{-1}$) and the dissipations only.

The relation between the spatial structure of the turbulence and the time variation of signals measured by stationary sensors are usually handled by appeal to Taylor's hypothesis of frozen turbulence. This hypothesis states that the temporal evolution seen by the sensor in average is due to the spatial variation of the turbulence field which is advected past the sensor by the mean wind, while the spatial field itself shows comparatively little variation. This means that an eddy of size ℓ will give rise to a variation in the time signal of a stationary probe over a time equal to $\ell/\bar{u}$ where $\bar{u}$ is the mean speed. Translated to the language of spectra this transforms to the following:

$$\begin{aligned} \omega = 2\pi f &= \bar{u} k_1 \\ k_1 S_1(k_1) &= \omega S(\omega) = f S(f) \end{aligned} \tag{14.10}$$

where the transformation characteristics of the spectral density function have been utilized and where k_1 is the component of the k-vector along the mean wind direction. The S_1-spectrum is found by integrating $S(k)$ over the other two k-components:

$$S_1(k_1) = \int_{-\infty}^{\infty} \int_{-\infty}^{\infty} S(\mathbf{k}) dk_2 dk_3 \tag{14.11}$$

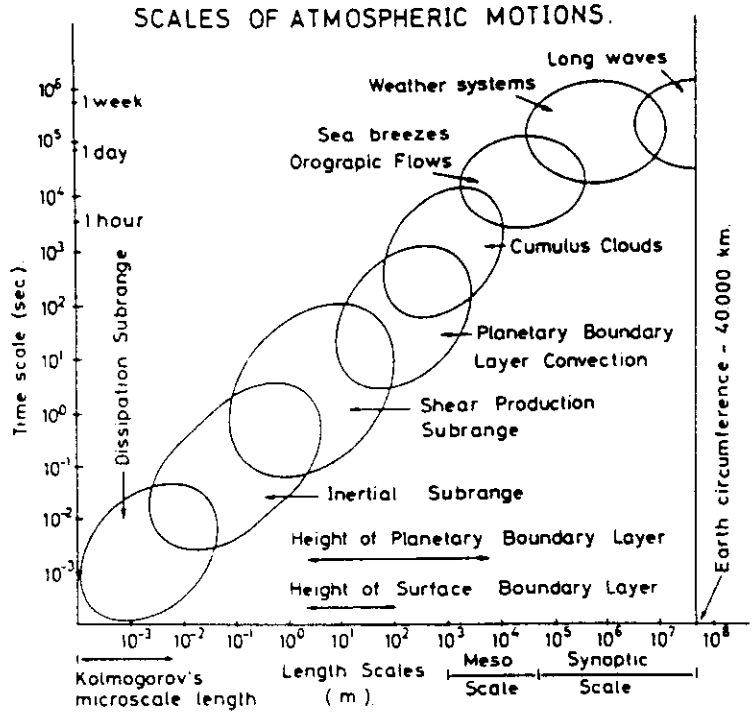

Figure 14.4: *Time and spatial scales for the processes influencing the flow in the atmospheric boundary layer (Busch et al., 1979).*

The spectral formulations and the Taylors hypothesis are based on quite simple ideas mainly of statistical nature and have been found to be so broadly valid that they are extremely useful in both experimental and modelling work. The practical limitations to the use of Taylor's hypothesis show when there is too much variation in the velocity relative to the mean flow, either due to turbulence or due to large vertical wind shear. This can influence the very low frequency, large-scale turbulence (Powell and Elderkin, 1974), and small-scale high frequency measurements (Wyngaard and Clifford, 1977, Mizuno and Panofsky, 1975). The limitation to the validity of the inertial subrange forms of the spectra is found when the assumption behind their validity breaks down, in the high-frequency end by the direct influence of the dissipation and in the low-frequency end through the direct showing of the production scales and the nearness of the surface.

Figure 14.4 presents a more general, but also more qualitative description of the spatial and temporal scales for the different processes influencing the flow in the atmospheric boundary layer. The figure directly shows the scale regions for the inertial subrange, while Taylor's hypothesis usually is used for time scales between 0.01 s and 1 h if the wind speed is not too small.

14.3 Basic equations, problems, and closures

The equation of state is described by the Ideal Gas Law:

$$p = \rho(R_0/M)T \tag{14.12}$$

where T is the temperature, ρ the density, M the molecular weight of the air and R_0 the universal gas constant. The atmosphere is a mixture of many different constituents. We shall concentrate on the most important gases, the *dry air* and the vater vapor. The water vapour and the dry air each exerts their partial pressure according to Eq. 14.12, thus:

$$p = \rho_d(R_0/Md)T + \rho_w(R_0/Mw)T \tag{14.13}$$

where ρ_d and ρ_w are the densities for the dry air and the water vapour, respectively.

Rearranging Eq. 14.13 we obtain

$$p = \rho R_d T_v \tag{14.14}$$

where R_d is the gas constant for dry air, $R_d = 287\ JK^{-1}kg^{-1}$, and Tv is a (the) virtual temperature, i.e. the temperature to be used in connection with the gas law to mimic the influence of water vapour if one wants to use the gas constant for dry air. It is defined by

$$T_v = T(1 + 0.61\,q) \tag{14.15}$$

where $q = \rho_w/\rho$ is the mixing ratio of water vapour in the air. The numerical coefficient derives from the ratio between the mole weights of dry air and water vapour.

Note that we have neglected the influence of the liquid water on the air density. This means that we cannot handle saturated air and thereby the boundary layer clouds that for some conditions can be quite important. Our excuse is that inclusion of the liquid water does complicate the equations quite a bit and that the role of the clouds is treated elsewhere in this book.

Having considered the influence of humidity we now turn to the height variation of the pressure, and introduce the potential temperature, θ, defined as the temperature an air parcel would attain if brought from its height, z, to some reference level usually taken at the sea surface. To a good approximation the vertical pressure distribution is controlled by the hydrostatic equation:

$$\partial p/\partial z = -\rho g \tag{14.16}$$

where g is the acceleration due to gravity. Since the pressure decreases with height, rising air parcels expand and sinking parcels compress. If the resulting vertical mixing takes place without

heat exchange, this equation can be combined with the first law of thermodynamics for adiabatic processes, $dp/dT = \rho c_p$ to yield the vertical temperature variation that would be in equilibrium with such a mixing. This gradient is normally called the adiabatic lapse rate for dry air and is denoted Γ and is found to be

$$-\partial T/\partial z = \Gamma = g/c_p \sim 0.01\,\mathrm{K/m} \tag{14.17}$$

Combining with the gas law, Equation 14.13, we can now solve the potential temperature at reference pressure, p_0

$$\theta/T = (p_0/p)^{R/c_p} \tag{14.18}$$

and

$$\partial\theta/\partial z = (\partial T/\partial z + \Gamma)\theta/T \tag{14.19}$$

If we use the surface as the reference level, then within the boundary layer $p \simeq p_0$ and $\theta \simeq T$. The vertical variation of θ is therefore given by

$$\theta(z) = T(z) + \Gamma z \tag{14.20}$$

Note that humidity has not been mentioned in this discussion meaning that R and c_p both depend on the water vapour mixing ratio, q and its height variation. Strictly speaking, therefore, the integration for humid air leading to Eq. 14.18 cannot be carried out. However, since R and c_p roughly vary the same way with q, their ratio is not very sensitive and one tends to use Eq. 14.20 for most boundary layer work except of course when clouds become involved. Strictly speaking however, Γ is seen to depend on q, compare Eq. 14.17 also for non-saturated air.

Neglecting the humidity influence on R/c_p in Eq. 14.18, we can define a virtual potential temperature as

$$\theta_v = \theta(1 + 0.61\,q) \tag{14.21}$$

corresponding to equation Eq. 14.15.

Next we proceed to the continuity equation:

$$\frac{\partial\rho}{\partial t} + \frac{\partial}{\partial x_j}\rho u_j = 0 \tag{14.22}$$

where summation over repeated indices is understood here and throughout the text. The coordinate system will be Cartesian with x_1, x_2, x_3 as the coordinates with the corresponding velocities u_1, u_2, u_3.

Within boundary layer meteorology the continuity equation is normally used in the incompressible form:

$$\frac{\partial u_j}{\partial x_j} = 0 \tag{14.23}$$

As seen this form corresponds to the assumption that the relative variations in density are much smaller than the variations in velocity and actually take some profound arguments about the relevant scales of variations for the variables (Businger, 1982). This will mainly be true for flows in the atmospheric boundary layer with scale lengths less than 10 km.

The conservation of momentum is normally used in the following form for the velocity component i in the atmospheric boundary layer:

$$\frac{\partial u_i}{\partial t} + u_j \frac{\partial u_i}{\partial x_j} = -g_i - f_c \epsilon_{ij3} u_j - \frac{1}{\rho}\frac{\partial p}{\partial x_i} + \nu \frac{\partial^2 u_i}{\partial x_j^2} \tag{14.24}$$

where f_c is the Coriolis parameter accounting for the motion to take place on a rotating planet. It is given as $f_c = 2\Omega \sin\phi$ where Ω is the angular frequency of the earth's rotation and ϕ is the latitude. At middle latitude f_c is of the order $10^{-4} s^{-1}$, g_i is zero for $i \neq 3$ and equal to the acceleration of gravity for $i = 3$. ϵ_{ijk} is the socalled alternating unit tensor being +1 if the subscripts are cyclic, -1 if not, and zero if two subscripts are equal. The kinematic viscocity is denoted ν, and as before p is pressure and ρ is the density. The equation shown in 14.24 has already been fairly strongly simplified from the basic Navier-Stokes equation in a rotating coordinate system. Equation 14.23 has been used repeatedly, we have neglected the effect of the rotation in the vertical component as well as other simplifications. It is easily recognized as Newton's second law for an air parcel: the right-hand side is the acceleration, while the left-hand side in the order of appearance is the forcing due to gravity, the effect of the rotating coordinate system, the forcing due to the pressure gradient, and the friction due to molecular forces.

At the same level of approximation as in Eq. 14.24 we can write the conservation of heat as

$$\frac{\partial \theta}{\partial t} + u_j \frac{\partial \theta}{\partial x_j} = k_T \frac{\partial^2 \theta}{\partial x_j^2} - LE/\rho c_p \tag{14.25}$$

where θ is the potential temperature defined in Eq. 14.20, k_T is the thermal diffusivity, E is the production of water vapour from water drops in the air, and L is the heat of evaporation. Relative to Eq. 14.24, Eq. 14.25 is seen to be vastly simpler, missing both the pressure and the Coriolis term. It does, however, couple to the budget for liquid water and humidity through the last term, both through E and through the fact that ρ and c_p pertain to the humid air. To further illustrate this coupling, we present below the budgets for the mixing ratios of liquid water, q_L, and for water vapour, q:

$$\frac{\partial q}{\partial t} + u_j \frac{\partial q}{\partial x_j} = k_q \frac{\partial^2 q}{\partial x_j^2} + E/\rho$$

$$\frac{\partial q_L}{\partial t} + u_j \frac{\partial q_L}{\partial x_j} = S_{q_L}/\rho - E/\rho \tag{14.26}$$

where k_q is the diffusivity of water vapour, E is the vapour production from evaporation, and S_{q_L} is additional local sources of liquid water by convergence of, e.g. spray produced from a water surface or rain drops falling down through the volume.

All of the equations are seen to possess one basic complication: they are nonlinear due to the advection term on the left-hand side. This nonlinearity is a general feature of fluid equation and is the origin of most of the complications one faces when trying to use these equations.

In section 14.2 the meaning of average values were discussed. As pointed out there, the ensemble averages were easiest to use when manipulating the equations. Based on the governing equations established above, we shall now establish the equations for the mean quantities. This is done by expanding all the variables in Eq. 14.23 through Eq. 14.26 into their mean values and fluctuating part, corresponding to Eq. 14.1. Inserting these expansions into the equation, averaging yields the equations for the mean quantities. When averaging the equations, all the fluctuating parameters will disappear except when entering nonlinear. The two important types of nonlinearity are the advection term on the right-hand side of all the equations and those involving the air density, ρ. Before generating the mean equations we shall therefore apply the Boussinesq approximation to remove the last of these nonlinearities. This approximation means letting $\rho'/\bar{\rho} \simeq 0$, except for the vertical component of the momentum equation, because here the mean pressure gradient and the mean density times gravity approximately cancel each other through the hydrostatic equation 14.16. From Eq. 14.24 with $i = 3$, we isolate the pressure and the gravity term and multiply $\bar{\rho}$ as:

$$\bar{\rho}(1 + \rho'/\bar{\rho})g - \frac{\partial}{\partial x_3}(p + \bar{p}') \simeq \rho' g - \frac{\partial p'}{\partial x_3} \tag{14.27}$$

The equation of state (14.14) can be expanded for small variations in the parameters as:

$$\frac{p'}{\bar{p}} = \frac{\rho'}{\bar{\rho}} + \frac{T_v'}{\overline{T_v}} + \frac{\rho' T_v'}{\bar{\rho}\overline{T_v}} \tag{14.28}$$

Considerations of the order of magnitude of the different terms, e.g. Businger (1982) and Stull (1988), yield:

$$-\frac{\rho'}{\bar{\rho}} = \frac{T_v'}{\overline{T_v}} \simeq \frac{\theta_v'}{\overline{\theta_v}} = \frac{\theta'}{\overline{\theta}} \tag{14.29}$$

where the last step uses the approximative relations between between θ_v and T_v within the boundary layer, compare Eq. 14.19 through Eq. 14.21.

Based on this discussion, we can now replace ρ by $\bar{\rho}$ everywhere in Eq. 14.24 through Eq. 14.26 and rewrite the momentum equation as

$$\frac{\partial u_i}{\partial t} + u_j \frac{\partial u_i}{\partial x_j} = -g_i \left(1 - \frac{\theta'_v}{\theta_v}\right) - \frac{1}{\bar{\rho}} \frac{\partial p}{\partial x_i} - \epsilon_{ij3} f_c u_j + \nu \frac{\partial^2 u_i}{\partial x_j^2} \tag{14.30}$$

Establishing the conditions for the validity of the approximations used above is not straightforward. It takes some pretty profound discussions of the scale of variability for the various terms in the equation. It is usually described as the shallow motion approximation or a somewhat more restrictictive shallow convection approximation (Mahrt,1986). It will *mostly* be fulfilled for scales of variability contained vertically within the boundary layer and horizontally within 15 km.

We now revert to the equations of the mean flow to obtain (Busch, 1973):

a) the continuity equation:

$$\frac{\partial \overline{u_i}}{\partial x_i} = 0 \tag{14.31}$$

b) the momentum equation:

$$\begin{aligned} \partial \bar{u}_i/\partial t + \overline{u_j} \frac{\partial \overline{u_i}}{\partial x_j} &= -g_i - f_c \epsilon_{i,j_3} - \frac{1}{\bar{\rho}} \frac{\partial \bar{p}}{\partial x_i} \\ &\quad + \nu \frac{\partial^2 \overline{u_j}}{\partial x_j^2} - \frac{\partial}{\partial x_j} \left(\overline{u_i' u_j'}\right) \end{aligned} \tag{14.32}$$

c) the heat or temperature equation:

$$\partial \bar{\theta}/\partial t + \overline{u_j} \frac{\partial \bar{\theta}}{\partial x_j} = k_T \frac{\partial^2 \bar{\theta}}{\partial x_j^2} - \frac{L\bar{E}}{\bar{\rho} c_p} - \frac{\partial}{\partial x_j} \left(\overline{u_j' \theta'}\right) \tag{14.33}$$

d) the equation for the water vapour mixing ratio:

$$\partial q/\partial t + \overline{u_j} \frac{\partial \bar{q}}{\partial x_j} = k_q \frac{\partial^2 \bar{q}}{\partial x_j^2} + \frac{\bar{E}}{\bar{\rho}} - \frac{\partial}{\partial x_j} \left(\overline{u_j' q'}\right) \tag{14.34}$$

Equations 3.21 through 3.23 show the socalled closure problem, i.e. the equations to derive the mean flow contain terms involving the statistics of the fluctuating components as well. Here $\frac{\partial}{\partial x_j}\overline{u_i' u_j'}$, $\frac{\partial}{\partial x_j}\overline{u_j' \theta'}$ and $\frac{\partial}{\partial x_j}\overline{u_i' q'}$. Physically these terms are gradients of turbulent fluxes of the different parameters. The covariance terms involving a velocity component describe fluxes as can be seen by considering the consequences for the flux of the x-parameter in the j-direction, of $\overline{u_j' x'}$ having a positive, negative or zero value. To close the set of equations, one must either prescribe the higher-order terms or relate them to the mean parameters already in the equations. One talks about closures of different order.

In zero-order closure the terms are prescribed by appeal to physical hypotheses. An example is the different similarity formulations to be described later.

In first-order closure the flux terms are characterized through the local gradient and a *turbulent* diffusion coefficient, normally denoted K. For example:

$$\begin{aligned} \overline{u_i' \xi'} &= K_{i\xi} \frac{\partial \bar{\xi}}{\partial x_i} \\ \overline{u_i' u_j'} &= K_{ij} \left(\frac{\partial \overline{u_i}}{\partial x_j} + \frac{\partial \overline{u_i}}{\partial x_i}\right) \end{aligned} \tag{14.35}$$

The K-diffusion concept is borrowed from the molecular gas theory that has given inspiration to how to determine K as well. In the molecular theory the diffusivity, k is found from expressions like (e.g. Chapman and Cowling, 1970):

$$k \sim (\text{ mean speed of the molecules }) \cdot (\text{ free path between molecular encounters}).$$

Following this idea we need a length and velocity scale for the turbulence to build a diffusivity. This is normally done by some combination of physical hypotheses and additional equations that can be used to determine these scales. The first efforts concentrated on the physical hyphotheses to prescribe K throughout the boundary layer. As an example of this approach can be mentioned the work of Businger and Araya (1974). When additional equations are carried to determine K, the simplest method used is to determine the equation for the variance of the turbulence velocity. Normally, this is called the energy equation because of the relation between the turbulence velocity and the turbulent kinetic energy. The standard deviation is then used as the velocity scale, and the length scale is derived using this velocity scale and the dissipation of turbulence energy, see Eq. 14.8, derived from a specially derived equation, see e.g. Arpaci and Larsen, 1984. This type of closure is normally called the $K - \epsilon$ closure and has been extensively used in connection with fluid modelling.

Strictly speaking, the $K - \epsilon$ closure is a type of higher-order closure because an equation for a second-order moment, the turbulence energy, is introduced to determine the diffusivity used to relate the covariance terms (second-order moments) in Eq. 14.32 through Eq. 14.34. The $K - \epsilon$ closure is often referred to as one and a half-order closure. A more strict type of higher-order closure is obtained by deriving equations for the covariances $\overline{u_j' u_i'}$, $\overline{u_j' \theta'}$ and $\overline{u_i' q'}$.

The equations for the fluctuating quantities can be generated by subtracting the equations for the mean flow, Eq. 14.32 through Eq. 14.34 from the basic equations, Eq. 14.24 through Eq. 14.26. To generate the equation for for a covariance say, $\overline{u_j' u_i'}$, we produce the equation for each of the fluxtuating quantities and note that

$$\frac{\partial}{\partial t}\overline{u_i' u_j'} = \overline{u_j' \frac{\partial}{\partial t} u_i'} + \overline{u_i' \frac{\partial}{\partial t} u_j'} \tag{14.36}$$

When producing the equations for the second-order moments so as to solve the equations for the mean flow, one will note that the equations generated contain third-order moments meaning that the closure problem will not go away. For these third order moments one can continue and generate

equations for the higher order moments as previously, or one can close with a diffusivity hypothesis, e.g.

$$\overline{u_i' u_j' \theta'} = K \left(\frac{\partial}{\partial x_i} \overline{u_j' \theta'} + \frac{\partial}{\partial x_j} \overline{u_i' \theta'} \right) \tag{14.37}$$

Solving the equations for both the mean values and the second-order moments has become quite a well-established technique, while including also the third-order equations is more rarely done. This is because of the difficulty in handling the number of equation, but also because many of the terms that appear in the higher-order equations are very difficult to relate to conceptually and even more uncertain to measure, see e.g. Wyngaard (1973, 1982).

We can summarize the disadvantages and advantages by the trying to close the equations by generating equations for the higher-order moments.

Disadvantages:

1. An ever increasing number of equations with associated boundary and initial conditions.
2. Eventually, one falls back on using the local K-diffusivity closure at the final order of equations. As stated above, the K-diffusivity for turbulence is an useful hyphothesis that is known not always to work, and it does not become more valid by being applied rather to higher-order moments than to second-order moments. Discussions and tests of validity just become more intransparent and difficult.

Advantages:

1. As results, one often wants the higher-order moments, e.g. all of the turbulence fluxes of momentum, heat, and water vapour are second-order moments.
2. By applying the K-diffusivity closure at ever higher-order moments, one might hope for larger generality because the higher-order moments get more and more determined by the structure of the small scale turbulence. Recall the simple picture in section 2 where the eddies gradually lose the memory of how they are produced when moving to smaller scales.
3. In spite of the principal criticisms that can be raised against the higher-order closure, it is a rational approach to solving the equations of motion that in extensive literature on the method and its results has shown its value.

Some of the shortcomings of the local closures have long been well-known: during the afternoon unstable boundary layer, the potential temperature can often be constant with height over the major part of the boundary layer. Under such conditions the vertical heat flux can be very strong, and therefore obviously does not follow a parameterization like Eq. 14.35. Correspondingly, it is well-known within air pollution meteorology that in its inital phase, the dispersion of a plume from a point source is inconsistent with the assumption of a diffusivity being a function of flow conditions

only. It would have to be a function of the distance from the source as well (Troen et al, 1980). This knowledge has led to efforts of repairing or replacing the local closure. In one approach, i.e. the transient turbulence theory (Stull,1988), the locality of the closure is given up, and the system simply specifies an exchange between non-neighbour air parcels according to certain rules. Another approach postulates that the diffusivity should be defined in Fourier space so that a diffusivity, $K(k)$, corresponds to each eddy-size or wave number, see Berkowicz and Prahm (1979), Troen et al (1980). Both systems work quite well with numerical codes and can be used when mean profiles of parameters are such that local closure gives wrong results. As the only caution one could say that they do not obviously give correct answers under all conditions. There is less empirical knowledge on how they perform in different situations than for the other closure systems that have been used much more extensively.

Finally, we turn to a modelling principle that is denoted Large Eddy Simulation or LES. Here the ensemble average, being the basic type of average when manipulating the equations above, is dropped for a spatial average more precisely defined. This has some advantages and some disadvantages as will be seen below.

The decomposition of signals is formally defined in the same way as in Eq. 14.1:

$$x = \{x\} + x' \tag{14.38}$$

where, however, the average value $\{x\}$ is now defined through some kind of spatial average over a volume that will typical correspond to a grid size, see e.g. Wyngaard (1982) :

$$\{x\} = \int_{-\infty}^{\infty} \int_{-\infty}^{\infty} \int_{-\infty}^{\infty} G(\mathbf{r} - \mathbf{r}') x(\mathbf{r}') \, d\mathbf{r}' \tag{14.39}$$

The equations for the average, $\{\cdot\}$, flow look very much like those of Eq. 14.31 through Eq. 14.34, but the second-order moments are now defined by:

$$\{x'y'\} = \{(x - \{x\})(y - \{y\})\} \tag{14.40}$$

with a closure equation of $\{u_i' y'\} = K_{iy} \frac{\partial \{y\}}{\partial x_i}$.

The main advantage of the LES modelling is that the scales of motion involved in $\{x\}$ and x' are much better defined than the normal Reynolds decomposition, where in principle all scales influence x'. The LES has a number of mathematical complexities, however. Both $\{x\}$ and x' are now stochastic functions, meaning that also K_{iy} is stochastic. A further estimation of $\{x'y'\}$ is more complex because $\{x\}$ and x' are now correlated through Eq. 14.36. In spite of these difficulties the techniques is becoming more and more used. This is because this model type can directly output the time and spatial variation of the larger eddies, those that are resolved by the model, while the models operating with ensemble averages by their nature can produce only ensemble averages of the different moments.

14.4 Simple Boundary Layers

In the former sessions we have generally used the coordinate system x_1, x_2, x_3 with associated wind speeds u_1, u_2, u_3. The only specifications of these coordinate systems have been that the 3-axis has been vertical. As we move down into simple boundary layers we shall more and more switch to a x, y, z coordinate system with associated wind speeds u, v, w. Here, x is along the mean wind close to the surface, meaning that u is the only wind component with a mean value; z is vertical and y is the other horizontal direction perpendicular to x.

To simplify the equations for the mean flow, Eq. 14.31 through Eq. 14.34, we define the geostrophic wind.

$$U_g = -\frac{1}{f_c\bar{\rho}}\frac{\partial \bar{p}}{\partial y} \qquad V_g = +\frac{1}{f_c\bar{\rho}}\frac{\partial \bar{p}}{\partial x} \tag{14.41}$$

Note that U_g is the component of the geostrophic wind along the mean wind direction at the surface. Inserting Eq. 14.5 into Eq. 14.29 through Eq. 14.32 and recalling that in this approximation $\bar{\rho}g \simeq \partial\bar{p}/\partial z$, the equations for the mean flow come out as:

$$\begin{aligned}
\bar{w} &= 0 \\
\frac{\partial \bar{u}}{\partial t} + \overline{u_j}\frac{\partial \bar{u}}{\partial x_j} &= -f_c(V_g - \bar{v}) - \frac{\partial}{\partial x_j}\overline{u_j' u'} \\
\frac{\partial \bar{v}}{\partial t} + \overline{u_j}\frac{\partial \bar{v}}{\partial x_j} &= f_c(U_g - \bar{u}) - \frac{\partial}{\partial x_j}\overline{u_j' v'} \\
\frac{\partial \bar{\theta}}{\partial t} + \overline{u_j}\frac{\partial \bar{\theta}}{\partial x_j} &= -L\bar{E}/\bar{\rho}c_p - \frac{\partial}{\partial x_j}\overline{u_j'\theta'} \\
\frac{\partial \bar{q}}{\partial t} + \overline{u_j}\frac{\partial \bar{q}}{\partial x_j} &= \bar{E}/\bar{\rho} - \frac{\partial}{\partial x_j}\overline{u_j' q'}
\end{aligned} \tag{14.42}$$

where we have neglected the molecular terms.

Equation Eq. 14.43 shows that if the left-hand sides are constant, then the two scalars will vary linearly with height, provided of course that we can neglect the E-terms.

The next step in simplifications comes when the left-hand side of Eq. 14.43 is assumed to be zero. In physical terms this corresponds to calling the flow statistically stationary and horizontally homogeneous. Eq. 14.43 now takes the form:

$$\begin{aligned}
\overline{w'\theta'} = \text{const.}\ \overline{w'q'} &= \text{const.} \\
-f_c(V_g - \bar{v}) - \frac{\partial}{\partial z}\overline{u'w'} &= 0 \\
f_c(U_g - \bar{u}) - \frac{\partial}{\partial z}\overline{v'w'} &= 0
\end{aligned} \tag{14.43}$$

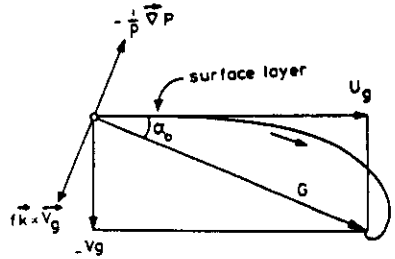

Figure 14.5: *The variation of the wind with height, taken from Tennekes (1982).*

The two equations in Eq. 14.44 can be closed with the type of K-diffusivity already discussed above, and one obtains a spiral-like variation of the wind with height as shown in Figure 14.5. It is often called the Ekman spiral, after the first proposer of this solution (Ekman, 1905).

The exact form of the spiral in Figure 14.5 will depend of course on the details of the closure used. In practice, however, one will often/mostly see a large deviation from the figure because the real world does not satisfy the stationarity and horizontal homogeneity assumption. Often one will find that horizontal temperature gradients induce vertical changes in the geostrophic wind, because under such condition. the hydrostatic equation (14.16) can not in generally be fulfilled with one constant $\bar{\rho}$. Also the curvature of the isobars, instationarity, and inhomogeneity will introduce changes in the equations, see e.g. Hasse (1976).

For the height, z, approaching zero, v goes to zero (because by definition only u can have a mean component close to the ground). From Eq. 14.44 we therefore conclude that:

$$\begin{aligned}
\partial\overline{u'w'}/\partial z &= -f_c V_g, \text{ or } \overline{u'w'} = \overline{u'w'_0} - f_c V_g z \\
\partial\overline{v'w'}/\partial z &= f_c(U_g - u(z))
\end{aligned} \tag{14.44}$$

where subscript 0 indicates surface value.

A closer inspection of the scales involved and the fact that the friction very close to the surface must be in the opposite direction of the mean speed implies that close to the surface we have:

$$\begin{aligned}
-\overline{u'w'} &= \overline{u'w'_0} = u_*^2 = \tau_0/\bar{\rho} \\
\overline{v'w'} &= 0
\end{aligned} \tag{14.45}$$

where we have defined the surface stress, τ_0, and the associated scale velocity u_*.

From the above we conclude that for stationary and horizontally homogeneous situations these exist close to the surface a layer, where also the turning of the wind and the change of stress with height can be neglected. The charactestics of this layer can be further illuminated by considering the equations

for the variances of the turbulent variations. Specifically the turbulent kinetic energy, $\bar{e} = \frac{1}{2}\overline{u_i'^2}$, $\overline{\theta'^2}$ and $\overline{q'^2}$. In section 3 we have already discussed how to produce equations for the covariances. The procedure is the same for the variances, just a bit simpler, because more terms can be contracted: For $\bar{e}$ we start with (3.19), and obtain after some manipulation:

$$0 = \frac{\partial \bar{e}}{\partial t} + u_j \frac{\partial \bar{e}}{\partial x_j} = -\overline{u'w'}\,\partial\bar{u}/\partial z + \frac{g}{\bar{\theta}_v}\overline{w'\theta_v'} - \frac{\partial}{\partial z}\left(\overline{w'\left(e + \frac{1}{\bar{\rho}}p'\right)}\right) - \epsilon \tag{14.46}$$

The $\overline{\theta'^2}$ and $\overline{q'^2}$ equations derive more easily from Eqs. 14.25 and 14.26, neglecting the E-terms.

$$\begin{aligned} 0 = \frac{\partial \overline{\theta'^2}}{\partial t} + \overline{u_j}\frac{\partial \overline{\theta'^2}}{\partial x_j} &= -2\overline{\theta'w'}\partial\bar{\theta}/\partial z - \frac{\partial}{\partial z}\overline{w'\theta'^2} - 2N_\theta \\ 0 = \frac{\partial \overline{q'^2}}{\partial t} + \overline{u_j}\frac{\partial \overline{q'^2}}{\partial x_j} &= -2\overline{q'w'}\partial\bar{q}/\partial z - \frac{\partial}{\partial z}\overline{w'q'^2} - 2N_q \end{aligned} \tag{14.47}$$

Here, ϵ, N_θ and N_q are the dissipations we have already met in section 14.2, and which we can now define from the equations as:

$$\epsilon = \nu\overline{\left(\frac{\partial u_i'}{\partial x_j}\right)^2},\ N_\theta = k_T\overline{\left(\frac{\partial \theta'}{\partial x_j}\right)^2},\ N_q = k_q\overline{\left(\frac{\partial q'}{\partial x_j}\right)^2} \tag{14.48}$$

In Eqs. 14.46 and 14.47 the terms on the right-hand side reflect the different sources and sinks for the turbulence. The first terms describe the production, P, of turbulent fluctuations through interaction between the turbulence and the shear of the mean flow. Dependent on its sign, the second term, B, in the equation for the kinetic energy describes the production or destruction of turbulent kinetic energy due to buoyancy. The last term in all of the equations has already been described in Eq. 14.48 as the dissipation of turbulent variations by molecular forces. Likewise, in all of the equations the last but one terms are called the divergence terms, D. They can be shown to redistribute the energy between different components of u_i as well as between different points in space.

Considerations of Eq. 14.45 through Eq. 14.47 have led to the idea that to describe the flow in the near-surface layer, one needs only to know the stress, heat flux, and water vapour flux together with the buoyancy parameter $g/\bar{\theta}_v$ and measuring height, z. Here, the latter is to account for the vertical gradients appearing in the equations. In the Monin-Obukhov scaling system these quantities have been combined to a number of scales that together describe the flow in the surface layer. They are:

$$\begin{aligned} u_* &= \left(-\overline{u'w'_0}\right)^{1/2} \qquad \theta_* = -\overline{\theta'w'_0}/u_* \\ q_* &= -\overline{q'w'_0}/u_* \qquad g/\bar{\theta}_v \quad \text{and} \quad z \end{aligned} \tag{14.49}$$

Note, that $\overline{w'\theta_v'} = \overline{w'\theta'} + 0.61\bar{\theta}\overline{w'\theta'}$, according to Eq. 14.21, θ_{v*} is defined accordingly. Some of these scales are combined to the stability scale, the Monin-Obuckov stability length, given by:

$$L = +\frac{\bar{\theta}_v}{g\kappa}u_*^2/\theta_{v*} \tag{14.50}$$

where κ is the socalled von Kármán constant that will later be introduced more rationally. As seen from Eq. 14.46 L can be considered as a ratio between the mechanical turbulence production and the buoyancy force. If the heat flux is positive, as on a sunny day with a warm suface, L is negative, and the situation is called unstable. On the other hand, if the heat flux is downward, as on a clear sky night with radiational cooling of the ground, L is positive. For both situations L increases with wind speed. L becomes largest, when the heat flux is very small, i.e. when the air and the ground are of roughly the same temperature. This situation is called thermally neutral and can be imagined as a situation with reasonably high wind and overcast sky, compare Figure 14.2. The arguments behind this scaling approach were originally introduced by Obukhov in 1943 in a paper that has been translated later on (Obukhov, 1971). The rule is that if any local turbulence statistics is non-dimensionalized with the parameters in Eq. 14.50, then the resulting non-dimensional groups will be functions of z/L only. Below this is illustrated on Eqs. 14.46 and 14.47 where the nondimensional functions are traditionally denoted ϕ and where the terms on the right-hand side appear in the same orders as in the original equations. Eq. 14.46 is multiplied by $\kappa z/u_*^3$ to give:

$$0 = \phi_m(z/L) - z/L - z/L\frac{\partial}{\partial\frac{z}{L}}\phi_D\left(\frac{z}{L}\right) - \phi_\epsilon(z/L) \tag{14.51}$$

Correspondingly, the two equations in Eq. 14.47 are multiplied by $\kappa z/(u_*\theta_*^2)$ and $\kappa z/(u_*q_*^2)$, respectively, to yield:

$$\begin{aligned} 0 &= 2\phi_h(z/L) - z/L\frac{\partial}{\partial\frac{z}{L}}\phi_{D\theta}\left(\frac{z}{L}\right) - 2\phi_{N\theta}(z/L) \\ 0 &= 2\phi_q(z/L) - z/L\frac{\partial}{\partial\frac{z}{L}}\phi_{Dq}\left(\frac{z}{L}\right) - 2\phi_{Nq}(z/L) \end{aligned} \tag{14.52}$$

The von Kármán constant, κ, is defined such that $\phi_m(z/L)$, the non-dimensional profile function, equals 1 for $z/L = 0$. ϕ_m, ϕ_h and ϕ_q are defined as

$$\phi_m(z/L) = \frac{\kappa z}{u_*}\frac{du}{dz} \qquad \phi_h\left(\frac{z}{L}\right) = \frac{\kappa z}{\theta_*}\frac{\partial\bar{\theta}}{\partial z},\ \phi_q\left(\frac{z}{L}\right) = \frac{\kappa z}{q_*}\frac{\partial\bar{q}}{\partial z} \tag{14.53}$$

The von Kármán constant must be experimentally determined and is found to be between 0.33 and 0.43 in different experiments. The other similarity functions defined in Eqs. 14.52 and 14.53 are the divergence functions, ϕ_D and the dissipation functions, ϕ_ϵ, ϕ_N.

Equation Eq. 14.52 illustrates how the buoyancy forces will produce turbulence for unstable situations, when L is negative, and destroy turbulence for stable conditions when L is positive.

The hypothesis about the surface boundary layer have been experimentally studied through a number of field experiments, starting with the wellknown Kansas 1968 experiment, from which the measuring set-up is shown in Figure 14.6.

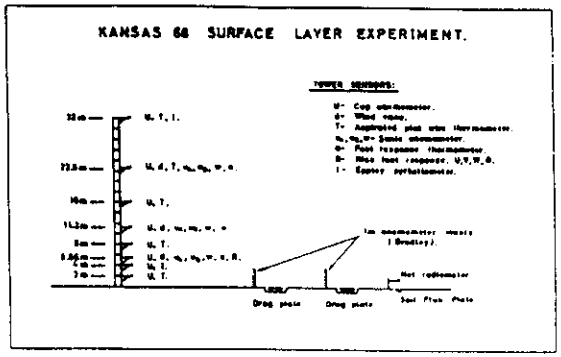

Figure 14.6: *Schematic presentation of the core instrumentation during the Kansas 1968 field experiment (Busch et al., 1979).*

Although first of its kind, the Kansas experiment is probably also the most complete surface-layer experiment carried out until today. In the context of the equations discussed above, the important missing parameters in the measuring program were humidity and pressure. As seen from the discussion above, the surface layer hyphoteses predict characteristics of the vertical variation of the mean values, fluxes, and their relation. Therefore the experiment was set up to measure mean values and turbulence at a number of heights with the turbulence (the most complicated) at three heights, the minimum number to measure the height variation of the divergence terms in the equations above.

From the Kansas experiment and its successors information has come on the behaviour of the different similarity funtions, some consensus both on the behaviour of the surface layer and on the limitation to its applicability, and some controversy that are still not properly resolved. Although controversy about the functions still exist, good qualitative agreement has been found between the different experiments (Businger et al., 1972; Wyngaard and Coté, 1972; Dyer, 1974; Högström, 1990). In Figure 14.7 is illustrated the results from such experiments.

The surface layer is only a small part of the total boundary layer. Its height is about 0.1 times the boundary layer height. Both because of this and because the surface layer studies showed that even here the parameters reflecting the total boundary layer were important for some quantities, the number of studies of all of the boundary layers increased since the early seventies.

The development in the description of simple boundary layers is best conducted seperately for the unstable, the neutral, and the stable boundary layer, with the stability being defined as in connection with the Eq. 14.49 through Eq. 14.52, and referring to Figure 14.2 for a qualitative picture.

As indicated by the name, the neutral boundary layer is controlled by mechanically produced turbulence, and the wind up through the boundary layer is described by Eq. 14.44, the height dependent balance between pressure force, Coriolis force, and the turbulent stress. The buoyancy term is unimportant. In its classical form the neutral boundary layer can be be very elegantly described by a similarity description, adding only the surface roughness to u_*, because the boundary layer height is considered to be given by the surface scale u_* and Coriolis parameter, see Tennekes (1973, 1982)

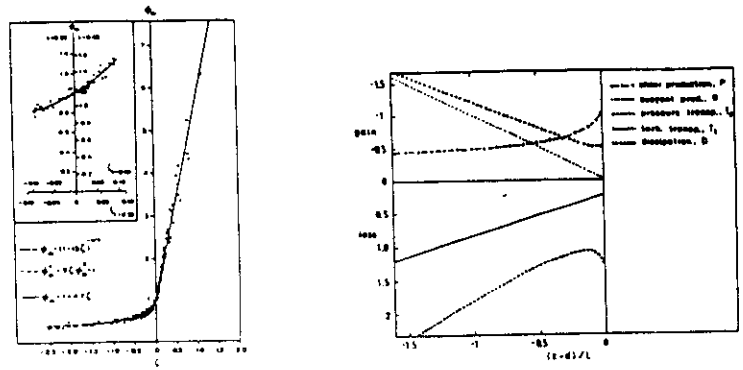

Figure 14.7: *Results from surface layer experiments. (a) shows the behaviour of ϕ_m versus $\xi = z/L$ from Businger et al 1971). (b) shows the relative importance of the different terms in Eq. 14.51 according to measurements by Högström (1990) and plotted versus $(z-d)/L$, where d is the displacement height to be defined later. In this Figure ϕ_D has been expanded into its turbulence T_t and its pressure T_p component.*

and Tennekes and Lumley (1982). In practice, however, also the neutral boundary layer height very often is controlled by the height of the first elevated inversion, at least at mid latitude. It must be emphasized that although the neutral boundary layer carries rather little sensible heat flux, it can be responsible for large water vapour fluxes, since the neutral boundary layer is often associated with large wind speed and thereby high turbulence mixing.

Unstable boundary layers are characterized by a strong positive heat flux and often a well developed capping inversion. They are fairly conveniently described by the strong vertical fluxes because the vertical mixing is of dominating importance. At the top of the unstable surface layer the production of turbulence from the mean shear becomes unimportant compared to the buoyancy production, compare Figure 14.2(a) and Eq. 14.51. This leads to the idea that the dominating velocity scale for the turbulence in the middle of the unstable boundary layer must be constructed from the surface heat flux and the the height of the boundary layer that constitute an upper limit for the size of the eddies carrying the fluxes. In the literature this height is called either z_i or h for unstable conditions. These ideas were supported by field, laboratory, and numerical experiments (Kaimal et al., 1976; Deardorff, 1970), and led to successful efforts to describe the turbulence in large parts of the unstable boundary layer by the following scales:

$$\begin{aligned} w_* = \left(z_i \overline{w'\theta'_{v0}}\, g/\bar{\theta}\right)^{1/3} &= u_*(-z_i/\kappa L)^{1/3} \\ T_* = -\overline{w'\theta'_0}/w_* \,,\; Q_* &= -\overline{q'w'_0}/w_* \end{aligned} \qquad (14.54)$$

h or z_i

The scales in Eq. 14.55 are usually denoted the mixed layer scales. Note that the fluxes used have to be evaluated at the surface, just as for the Monin-Obukhov scales. The mixed layer scales can be used

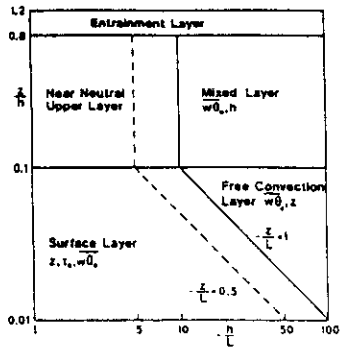

Figure 14.8: *The different scaling regions in the unstable boundary layer according to to Holtslag and Nieuwstadt (1986).*

to scale the equation of motion, just as the Monin-Obukhov scales were used in Eq. 14.51 through Eq. 14.53. The similarity functions are often called ψ and are functions of (z/h) corresponding to ϕ in the surface layer, and as an aesthetic advantage the mixed layer scales do not involve an emperical constant like the von Kármán constant in the surface layer scales. A systematic description of the turbulence equations in the mixed layer is given in Stull (1988).

In between the mixed layer and the surface layer is a matching layer where both the surface layer and the mixed layer scalings are supposed to work. This is called the matching layer or the free convection layer. It is a layer where the velocity shear is unimportant as in the mixed layer, but where also the height of the boundary layer is unimportant as in the surface layer. Based on these considerations, a number of rules can be derived for the behaviour of the turbulence statistics in the stronly unstable surface layer (Wyngaard and Coté 1971). Given the proliferation of scaling regimes in the boundary layer, several authors have tried to present systematic descriptions as to when and where the different scaling regimes apply (Nicholls and Readings, 1979; Olesen et al., 1984; Holtslag and Nieuwstadt, 1986). Figure 14.8 shows the organization of the scaling regimes in the unstable boundary layer from the latter authors.

Apart from the scaling regions discussed above, Figure 14.8 shows two new regions. The near-neutral upper layer that cannot easily be simplified. This is because here all scales retain their importance. The entrainment layer around the top of the boundary layer, through which the boundary layer interacts with and entrains air from the free atmosphere above (Zilitinkevich, 1991).

Studies have shown that in many ways the top of the boundary layer appears as a surface layer turned upside down, e.g. the scale of turbulence decreases when one approaches the entrainment zone, much in the same way as it decreases when approachindg the surface. This led Wyngaard and Brost (1984) to suggest that through the unstable boundary layer the vertical diffusion of passive scalars can be computed as a superposition of top-down and bottom-up components driven by the scalar fluxes at the bottom of the boundary layer and at the mixed layer top, respectively. For example the vertical concentration gradients and fluxes of x can be represented by:

$$\begin{aligned} \bar{x} &= \bar{x}_b + \bar{x}_t \\ \frac{\partial \bar{x}}{\partial z} &= \frac{\partial \bar{x}_b}{\partial z} + \frac{\partial \bar{x}_t}{\partial z} \\ \overline{x'w'} &= \overline{x'w'_h} \cdot z/h + (1 - z/h)\overline{x'w'_s} \end{aligned} \tag{14.55}$$

The gradients of $\bar{x}_b$ and $\bar{x}_t$ each scale with their version of the mixed layer scaling:

$$\frac{\partial \bar{x}_b}{\partial z} = \frac{-\overline{w'x'_s}}{w_* h} g_b\left(\frac{z}{h}\right) \ , \ \frac{\partial \bar{x}_t}{\partial z} = -\frac{\overline{w'x'_h}}{w_* h} g_t\left(\frac{z}{h}\right) \tag{14.56}$$

where the two functions must be constructed taking into account the similarities and differences between the turbulence processes at the surface and at the top of the boundary layer, see Wyngaard and Brost (1984).

Recall the discussion in section 14.3 about use of K-diffusivity and local closure in the unstable boundary layer when the vertical gradient was zero. It is seen that this problem has been avoided with this superposition, because each of the gradient $\partial \bar{x}_b/\partial z$ and $\partial x_t/\partial z$ are non-zero. The approach has been used with some succes, exactly in situations where the gradient was zero (Fairall, 1987).

Finally, we turn to the stable planetary boundary layer. It is characterized by negative heat flux, often low velocity, and reduced turbulence activity, both due to buoyancy damping and low velocity. As opposed to the unstable boundary layer, real stable boundary layers are not easy to model, because the vertical fluxes are small, and other processes, like radiation balances and advection, therefore important. In terms of Eq. 14.51 we see that as stabilty increases, z/L will eventually become so large that the loss terms in the equation will overcome the production term, ϕ_m, and the turbulence will cease. This argument can be further illustrated by the behaviour of the Richardson numbers. The flux Richardson number is built as the ratio between the two first terms on the right hand-side of Eq. 14.46

$$Rf = \frac{g}{\theta_v} \frac{\overline{w'\theta'_v}}{\overline{u'w'}\frac{\partial u}{\partial z}} \tag{14.57}$$

From Eq. 14.46 is seen that turbulence is unlikely to exist when Rf becomes of the order of or exceeds one. Since Rf contains a mixture of turbulence and mean value gradient terms it was earlier fairly difficult to estimate experimentally this quantity. Therefore, gradient Richardson number, Ri, was formulated:

$$Ri = \frac{g}{\theta_v} \frac{\partial \bar{\theta}_v}{\partial z} \Big/ \left(\frac{\partial \bar{u}}{\partial z}\right)^2 \tag{14.58}$$

The relation between the two Richardson numbers is obvious, but as seen Ri can be determined from measurements of profiles of mean values only. In both theoretical and experimental studies Ri has been found to have a critical value, Ri_c, above which continuous turbulence cannot exist. The value

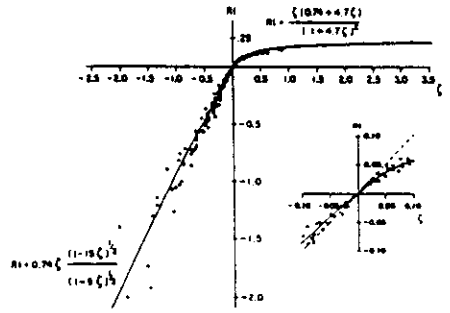

Figure 14.9: *The relation between the Richardson number and $\xi = z/L$ from (Businger et al., 1971).*

for Ri_c is generally found to be between 0.15 and 0.3 in most studies. From a theoretical point of view the value will depend on both how one relates Ri to Rf and on how the other two terms in Eq. 14.46 are estimated. From the experimental studies we present the relation between Ri and z/L from the Kansas experiment where the data seem to show a critical value around 0.2

As the stability increases, the surface layer scaling laws take a special form, called the z-less. This can be illustrated from the behaviour of the ϕ_m function reported in Figure 14.7(a). On the stable side it is seen to vary linearly with z/L, say as $1+ 5\ z/L$ (Dyer, 1974). From the definition of ϕ_m the consequence of this form is that for large z/L, $\bar{u}/z$ becomes independent of z. Many of the other local turbulence characteristics show this behaviour, hence the name (Wyngaard, 1973).

These characteristics of the stable boundary layer led Nieuwstadt (1984) to suggest a similarity model for the stable boundary layer based on the assumption that $Rf = Ri = Ri_c$ and that the turbulence would scale with the local fluxes, not the surface values of the fluxes as in the the Monin-Obukhov and mixed layer similarity but the local values. This necessitated estimates of the height variation of stress and heat flux relative to the surface values, such that the flow in the entire boundary layer could be computed. The local scaling parameters are normally related to the surface values from expressions like:

$$\begin{aligned} \tau^{1/2}/u_* &= (1 - z/h)^{\alpha_1}\ ,\ \overline{w'\theta'}/\overline{w'\theta'}_0 = (1 - z/h)^{\alpha_2} \\ \Lambda/L &= (1 - z/h)^{\alpha_3} \\ \Lambda &= \frac{\theta_*}{g\kappa}\tau^{3/2}/\overline{w'\theta'} \end{aligned} \tag{14.59}$$

As seen Λ is a Monin-Obukhov length determined from the local fluxes. As $\Lambda \to L$ for $z \to 0$, the local scaling and the surface layer scaling overlap for small z. The α-values can be estimated from measurements or closure hypotheses. Although complete consensus is missing, they are all of the order one (Caughey, 1982).

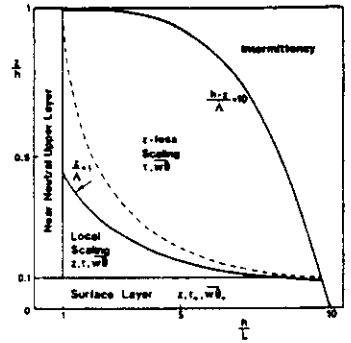

Figure 14.10: *Scaling regimes in the stable boundary layer according to Holtslag and Nieuwstadt (1986) based on the scaling parameters discussed in this section. The dashed line is given by $z/L = 1$.*

Corresponding to Figure 14.8 for the unstable boundary layer, we finally present a figure of the different scaling regions for the stable boundary layer in Figure 14.10, also taken from Holtslag and Nieuwstadt (1986).

Figure 14.10 shows a region denoted *intermittency*. In this parameter region the Richardson number is close to or larger than a crtical value for which reason continuous turbulence cannot exist. The fluxes in this region are believed to be carried by intermittet turbulence events, either induced by shear instability or internal gravity waves.

In the next sections we shall discuss the upper and lower boundary condition for the boundary layers. Here we just note that use of the z/h parameter in Figures 14.8 and 14.10 camouflages the large variability of the boundary layer height for the different situations with typical values of $h = 1000\ m$ for the unstable to neutral cases, and $h = 100\ m$ for stable cases and, as said, with huge variations.

14.5 Conditions at the surface

The similarity expressions in Eq. 14.53 can be integrated to the profiles of wind speed, temperature, and humidity:

$$\begin{aligned} \bar{u}(z) &= u_*/\kappa \left(\ln\left(\frac{z-d}{z_0}\right) - \psi_m\left(\frac{z-d}{L}\right)\right) \\ \bar{\theta}(z) - \theta_0 &= \theta_*/\kappa \left(\ln\left(\frac{z-d}{z_{0T}}\right) - \psi_h\left(\frac{z-d}{L}\right)\right) \\ \bar{q}(z) - q_0 &= q_*/\kappa \left(\ln\left(\frac{z-d}{z_{0q}}\right) - \psi_q\left(\frac{z-d}{L}\right)\right) \end{aligned} \tag{14.60}$$

where the d is a zero plane height called the displacement height, the ψ-functions are related to the ϕ-functions through:

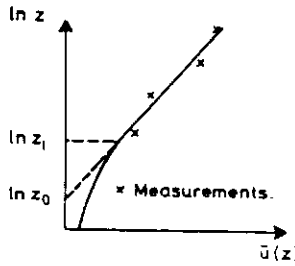

Figure 14.11: *Extrapolation of the wind profile to zero wind speed to obtain z_0. The lower height of validity for the neutral logarithmic law is denoted z_l.*

$$\psi\left(\frac{z-d}{L}\right) = \int_0^{(z-d)/L} (1-\phi(x))\frac{dx}{x} \tag{14.61}$$

All of the functions in Eq. 14.61 approach zero for $(z-d)/L \to 0$ so that Eq. 14.61 shows the profile approach to the logarithmic form for neutral conditions. Note that the z/L formulation of stability means that a boundary layer always tends towards neutral close to the surface, and that a boundary layer that appears neutral at the surface can turn more and more non-neutral as z and thereby z/L grow. Here, the different *roughness* lengths, z_0, z_0T and z_0q, are introduced formally as the heights where the surface layer forms attain the true surface values. As seen this gives a simple way of estimating z_0 as illustrated in Figure 14.11 where the measured wind profile is extrapolated down to the height z_0 where the wind speed is zero. It is worth pointing out that this method does not work so easily for the temperature and humidity profiles because surface values of these parameters are not so well-known as those for the wind speed where it is zero.

In Eq. 14.61 we have introduced the displacement height as well. If the the zero level is obviously well defined, d is of no use. But for many studies of very rough terrain like woods and built-up areas, the zero level is not well defined and it is an advantage to have d as a semi-free parameter when fitting profiles. Theoretically, the displacement height can be defined as the level at which the mean drag on the surface appears to act, and formulas for d can be worked out for specified surfaces (Jackson, 1981).

The lower height of validity for the turbulence surface layer profiles, z_l, is usually determined emperically as $10-30$ times z_0 or for canopies $3-6$ times the height of the vegetation (Garrat, 1978; Raupach, 1979).

The method in Figure 14.11 is often not available, and z_0 must be otherwise estimated, usually based on physical considerations on, e.g. what the surface actually does to the flow, combined with the available data on the roughnesses from different measurements. As we get close to the surface we leave the surface layer as defined in section 4, and the turbulence reduces too much to carry all the momentum nessecary to brake the flow to zero velocity at the ground. Equation Eq. 14.32 shows that the braking must be done by the molecular friction or by the pressure term due to form drag on the individual obstacles constituting the surface, i.e. the roughness elements. For surfaces where the roughness elements appear as individual distinct elements, the formula of Lettau (1969):

$$z_0 = 0.5HS/A \tag{14.62}$$

Here a roughness element is characterized by its height, H and the cross wind area, S. The density of roughness elements are described by the average area available to each element, A. The equation gives reasonable estimates of z_0 when A is much larger than S, but tends to overestimate z_0 when A is of the order of S. This is because the roughness elements also contribute to a displacement height not included in the equation (Troen and Petersen, 1989). For water surfaces one will often use the Charnock (1955) relation:

$$z_0 = cu_*^2/g \tag{14.63}$$

where c is a *constant* of the order of 0.012-0.02. Equation 14.63, however, is found to describe the roughness over sand surfaces as well.

Extensive work has been done for crop covered fields, to relate d and z_0 to the vegetation characteristics and to describe the flow and flux conditions above and within the canopy (Thom, 1971; Brutsaert, 1975; Brutsaert, 1982). The relations between vegetation height, displacement length, and roughness are often presented as:

$$z_0 = \lambda(H-d) \tag{14.64}$$

with d of the order $2/3$ H and λ of the order of $1/3$.

In the literature many of the roughness studies finally end up in figures that could be called the accumulated conventional wisdom method for determining the roughness for a given terrain. In Figure 14.12 we present one of the latest of such figures.

Roughness estimates from figures like Figure 14.12 have been found to work quite well when used to estimate the local wind speeds for the purpose of wind energy production (Troen and Petersen, 1989). Although the figure does indicate the existence of seasonal variation of z_0, it is worth emphazising that for vegetated surfaces the roughness must be expected to show some variation with the vegetation growth cycle. This is illustrated in Figure 14.13 that shows the average seasonal variation in z_0 from three nearby fields in Denmark.

Sofar we have discussed mostly the aerodynamic roughness. Similar to z_0, the scalar roughnesses, z_{0T} and z_{0q}, are associated again with a logarithmic profile and the fluxes for a given vertical mean gradients. Hence, the magnitude of the different z_0's is controlled by transport mechanisms very close to the surface where molecular processes are important. Since the processes driving the scalar fluxes lack the mechanism of form drag around the roughness elements, that is available for the transfer of momentum, the scalar z_0's are generally less than z_0.

As an example, consider the two-layer heat flux model in Figure 14.14.

The Figure shows an upper turbulent surface layer (I) and a lower interfacial layer (II) where the heat flux is carried by molecular transport. Equating the flux in the two layers:

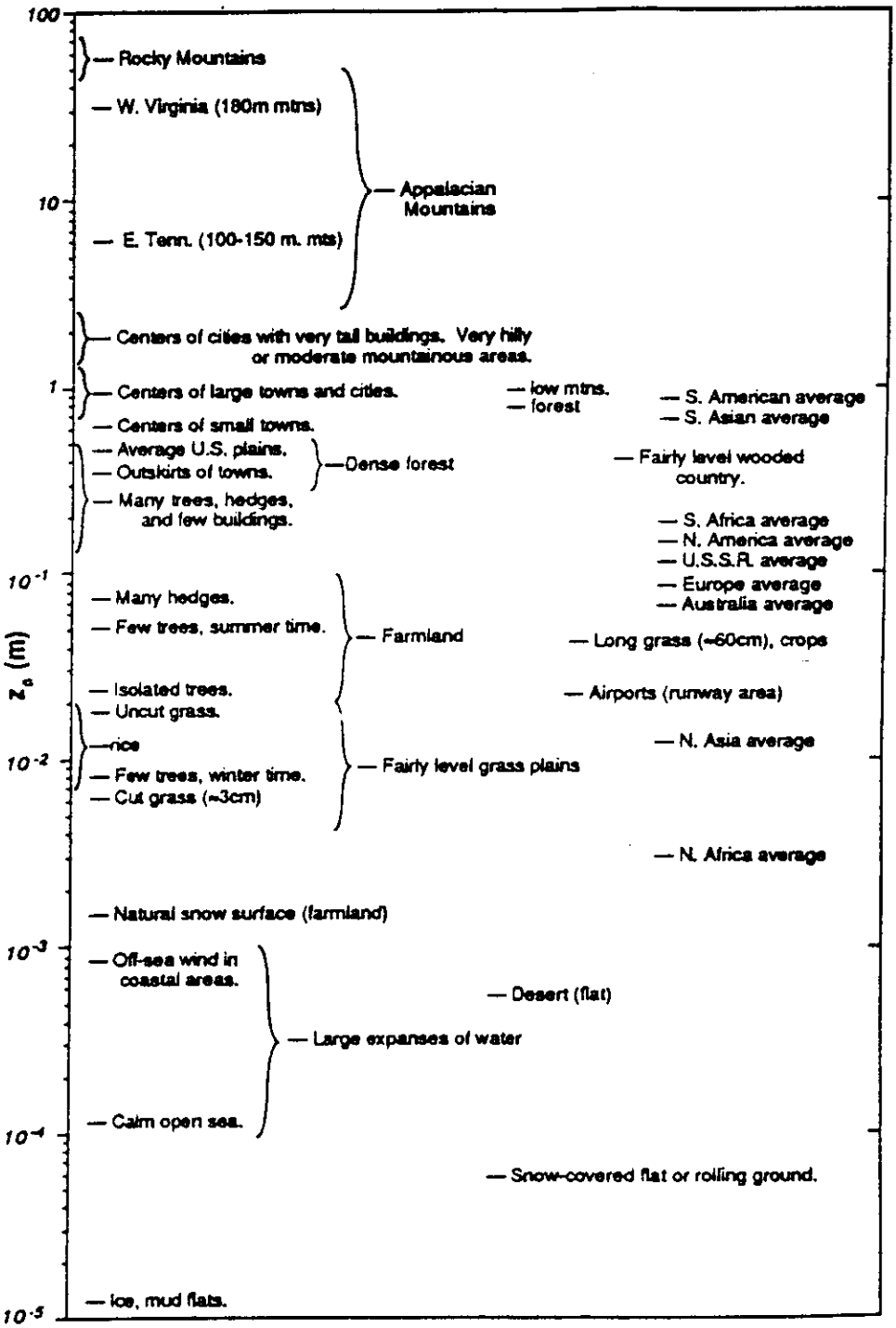

Figure 14.12: *The aerodynamic roughness length in different terrain types (Stull, 1988) integrating many earlier figures.*

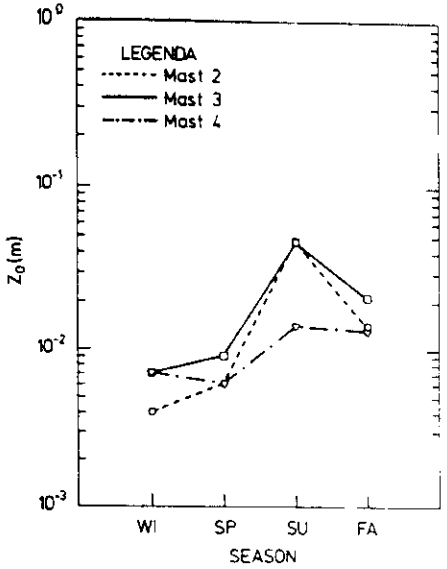

Figure 14.13: *Average seasonal variation of z_0 from two years of data at three nearby fields in Denmark (Sempreviva et al., 1989).*

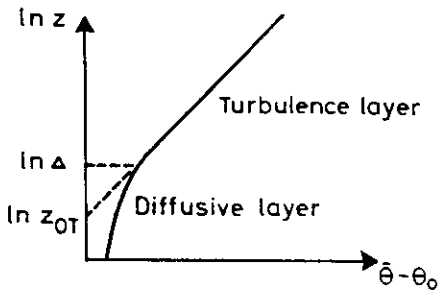

Figure 14.14: *A two-layer heat flux model to relate z_{0T} to z_0 (Jensen, 1991). The height Δ is the intersection height between the two layers.*

$$\begin{aligned} \text{(I)} - H &= \kappa u_* \left(\tilde{\theta_\Delta} - \theta_0\right) / \ln\left(\Delta / z_{0T}\right) \\ \text{(II)} - H &= k_T \left(\theta_\Delta - \theta_0\right) / \Delta \end{aligned} \tag{14.65}$$

which leads to $\ln(z_0/z_{0T}) = \kappa X$, with X given by $X = \Delta \frac{\kappa}{k_T} u_* - \ln(\Delta/z_0)$. X is usually presented as a function of the roughness Reynolds number, $Re_0 = u_* z_0/\nu$ and the Prandl number, $Pr = \nu/k_T$ for temperature, or the Scmidt number for humidity, $Sc = \nu/k_q$.

Many formulations are proposed in literature. We present the following from Brusaert (1982):

$$X(Re_0, Pr/Sc) = 7.3 Re_0^{1/4} Sc^{1/2} \tag{14.66}$$

where Pr is used for z_{0T} and Sc for z_{0q}. For a fairly wide range of atmospheric conditions this yield that the scalar roughnesses are about 0.1 z_0. The formulation used here is not applicable for fibrious surfaces, but also here the scalar roughnesses are found to be about 0.1 z_0. It would be nice to finish this section by specifying how to estimate θ_0 and q_0. in Eq. 14.61. From a modelling point of view this will obviously take estimates of the heat and moisture flux both above the surface and below in the vegetation and the soil. Also direct measurements are difficult, among others reasons because the surface in the sense of Eq. 14.61 is not necessarily very well physically defined. In spite of this, the surface radiation temperature for different surfaces has been used to test the z_{0T} expressions discussed above. In principle the surface parameters can be estimated from mesured profiles of $\tilde{\theta}(z)$ and $\tilde{q}(z)$ by extrapolating these down to z_{0T} and z_{0q}, if one believes in the methods for determining these parameters and the displacement height.

14.6 The upper boundary

In the three former sections the characteristics of the boundary layer flows and fluxes have been considered in terms of scales and relations defined within the boundary layer itself. One of the objectives is to describe fluxes through the boundary layer for given conditions at the surface and in the free atmosphere. Therefore we need to relate the boundary layer scales to the conditions in the free atmosphere above the boundary layer.

As a reasonable starting point we choose Eq. 14.44 because this equation contains the geostrophic wind, i.e. the wind above the boundary layer. For ideal neutral boundary layers these equation can be shown to lead to (Tennekes, 1982):

$$\begin{aligned} \kappa U_g/u_* &= (\ln(h/z_0) - A), \qquad \kappa V_g/u_* = -B, \\ h &= u_*/f_c, \qquad A \text{ and } B \text{ constants} \end{aligned} \tag{14.67}$$

It has been found from data that $A \sim 2$, while $B \sim 5$.

Equation Eq. 14.67 is called the *Resistance Law* for the neutral boundary layer because it describes the friction measured as u_*, exerted from the surface on the free stream flow. Substantial theoretical and experimental efforts have gone into generalizing Eq. 14.67, both to more general conditions and to scalar fluxes as well (Zilitinkevich, 1972 and 1975; Clarke and Hess, 1974; Melgarejo and Deardorff, 1974; Hasse, 1976; Araya, 1978):

$$\begin{aligned} \kappa U_h/u_* &= \ln(h/z_0) - A(\mu), \qquad \kappa V_h/u_* = -B(\mu) \\ \theta_h - \theta_0 &= \theta_*(\ln(h/z_{0T}) - C(\mu)) \\ \mu &= u_*/f_c L \text{ or } u = h/L \end{aligned} \tag{14.68}$$

In principle, the corresponding equation from humidity can easily be constructed from the temperature equation.

The stability parameter μ is the ratio between the boundary layer height and the Monin-Obukhov length.

Often the velocity resistance law is seen formulated in terms of the geostrophic wind speed and the angle between the surface wind and the geostrophic wind, $G^2 = U_h^2 + V_h^2$. From Eq. 14.69 the relation for G becomes:

$$\kappa G/u_* = ((\ln(h/z_0) - A(\mu))^2 + B^2(\mu))^{1/2} \tag{14.69}$$

In Figure 14.15 the stabilty functions $A(\mu)$ and $B(\mu)$ are presented. The scatter is seen to be substantial and characteristic for these types of plots. The scatter is not only in the data, also the model varies considerably among authors, some prefer μ based on the actual boundary layer height, some that it is based on u_*/f_c. Some authors prefer to use the surface geostrophic wind while others use the actual wind for $z = h$. Also several methods have been suggested on how to include the effects of instationarity, advection, baroclinity, etc. (Zilitinkevich, 1975; Hasse, 1976; Araya, 1978).

Not neglecting the uncertainty and scatter associated with the resistance laws, the neutral versions have been found to work very well for the moderate to high wind relevant for wind energy purposes (Troen and Petersen, 1989). Here data from 120 meteorological stations in Northwestern Europe were predicted from each other using Eq. 14.67 as the description of the wind above the boundary layer.

As discussed above, the initial estimate for the height of the boundary layer was formulated as:

$$h \sim c u_*/f_c \tag{14.70}$$

where c is normally choosen between 0.1 and $c = \kappa$. This expression does describe the data, although not overwhelmingly good. Also neutral boundary layer height is controlled, not only by u_*/f_c, but also by the strength and position of the lowest elevated inversion.

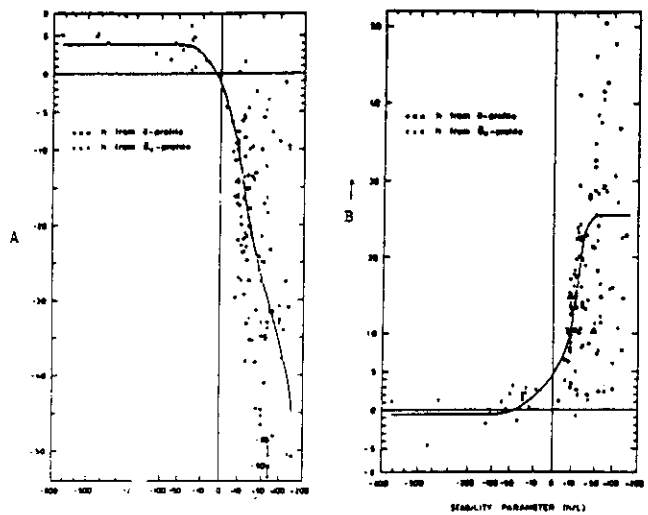

Figure 14.15: *The two stability funtions $A(\mu)$ and $B(\mu)$ as functions of h/L according to Melgarejo and Deardorff (1974).*

Such an expression can be found from the oceanographic modelling of the *inverse* problem, the depth of the mixed layer (Pollard et al., 1973)

$$h = 2^{3/4}\left(frac u_*^2 f_c N\right)^{1/2} \tag{14.71}$$

where N is the Brunt-Vaisala frequency, here used to describe the temperature stratification just outside the boundary layer.

$$N = \left(\frac{g}{\bar{\theta}}\frac{\partial \bar{\theta}}{\partial z}\right)^{1/2} \tag{14.72}$$

As a typical value of N in the free atmosphere is about 0.025 s^{-1}, Eq. 14.71 implies a value of $c \sim 0.15$ in Eq. 14.70 at midlatitude with $f_c \sim 1.5 \cdot 10^{-4} s^{-1}$.

Formulas for the height of the stable boundary layer have been worked out as well (Zilitinkevich, 1972) with:

$$h = C(u_* L/f_c)^{1/2} \tag{14.73}$$

with C around 0.7 (Caughey, 1982). The formulation simply suggests that the boundary layer height is the geometric mean between the neutral heigh, u_*/f_c and the Monin-Obukhov length.

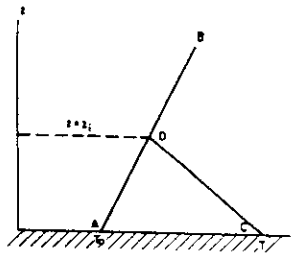

Figure 14.16: *Illustration of how the boundary layer height, $z_I = h$, grows when at sunrise the atmosphere is heated from belowe. The AB-curve represents the temperature profile at sunrise, CDB the profile after surface heating and entraining from aloft has warmed the lower layer (Panofsky and Dutton, 1984).*

For the unstable boundary layer it became obvious that formulas as the above could not be made to function. Therefore, quite soon it was proposed to determine the unstable h from a prognostic equation (Deardorff, 1972 Zilitinkevich, 1975). Consider Figure 14.16.

In Figure 14.16 we denote the temperature gradient at sunrise, line AB, as $-\gamma_n$, the gradient within the heated layer as $-\gamma_d$. γ is noramlly denoted the lapse rate. The night time gradient is likely to correspond to some type of stable situation, while the day time gradient will be close to adiabatic. Geometry then yields:

$$\gamma_d - \gamma_n = (T - T_0)/h \tag{14.74}$$

The conservation of heat yields, including both the heat flux from the surface and from the top:

$$\overline{w'\theta'_s} - \overline{w'\theta'_h} = (T - T_0)/h \tag{14.75}$$

Combining these two equations and differentiating, we obtain:

$$h\frac{\partial h}{\partial t} = \overline{w'\theta'_s}(1 + A)/(\gamma_d - \gamma_n) \tag{14.76}$$

where we have included the heat delivered to the boundary layer from the free atmosphere as a fraction, A, of the surface heat flux, usually taken as approximately 20 per cent. The equations are solved to yield:

$$h(t) = (2\int_0^t \overline{w'\theta'_s}(1 + A)dt/(\gamma_d - \gamma_n))^{1/2} \tag{14.77}$$

The rate equation for the unstable boundary layer gives quite satisfactory results. It has been much further developed and yielded a very satisfactory comparison with data on the growth of the unstable bounday layer, e.g. Gryning and Batchvarova (1990).

The development within the field is concentrated around improved description of the entrainment at the top of the boundary layer and the associated flux. The parameterization involves the structure of the entrainment zone that is as wide or wider than the boundary layer. The entrainment zone is physically described as a region where plumes and billows raise through a stable background air, with different types of turbulence and waves being generated on the interfaces (Tennekes and Driedonks, 1980; Zillitinkevich, 1991). The entrainment is often described in terms of an entrainment velocity ,w_e, defined by:

$$\overline{w'\theta'_h} = w_e\Delta\theta(EZ) \tag{14.78}$$

where $\Delta\theta(EZ)$ is the temperature gradient across the entrainment zone that is between the free atmosphere and the boundary layer. A general equation for the boundary layer height is often formulated as:

$$\partial h/\partial t = -u_j\partial h/\partial x_j + w_s + w_e + w_{ls} \tag{14.79}$$

where also advection of boundary layers with generated heights other than the local. w_s and w_e are the rise induced by the local fluxes as given by Eq. 14.76, while w_{ls} reflects larger scale movement of the atmosphere as, e.g. subsidence. Note that Eq. 14.79 allows for stationary unstable boundary layer heights.

At least for scalars the entrainment constitutes an alternative to the resistance laws to relate the conditions within the boundary layer to the conditions outside, compare Eq. 14.78 where the conditions in the free atmosphere enter through $\Delta\theta(EZ)$. For any scalar x, we can of course generate an equation like Eq. 14.78. Also note that the top-down part of the bottom-up/top-down description of the unstable boundary layer in Eqs. 14.56 and 14.56 includes the entrainment.

Finally, it should be mentioned that the success of the rate equations for the height of the unstable boundary layer has let to similar but less successful efforts for the stable boundary layer. This is due mainly to the absence of strong dominating verical fluxes here.

14.7 Demands to measurements

The plans for a measuring campaign in the atmospheric boundary layer can be organized in many ways. Below we shall try to organize the relevant points, as:

1. temporal and spatial scales that should be resolved
2. statistical demands to the data
3. instrumentation technology, calibration problems, and flow distortion.

For a simple homogeneous boundary layer average flow changes takes place only in the vertical dimension. If one can use several measuring heights, the levels should be more close at the bottom than heigher up due to the form of the profile functions as discussed in sections 4 and 5. If possible one should try to measure fluxes directly from turbulence measurements. Fluxes can be estimated from profile measurements, as can be seen from Eq. 14.61. However, both measuring uncertainties and the uncertainty about the value of the von Kármán *constant* point towards a direct measuring of the turbulence fluxes.

In the surface layer, it follows from Eq. 14.61 and the discussion about the behaviour of the ϕ-functions that profiles for a fairly large stability interval around neutral can be written as:

$$x(z) = a + b\ln(z) + cz \tag{14.80}$$

where the , b, and c coefficients contain all profile parameters other than z. If measurements of Eq. 14.80 are conducted in the two heights, z_1 and z_2, the measured gradient will correspond to $\partial\bar{x}/\partial z$ at the height $z = (z_2 - z_1)/\ln(z_2/z_1)$ as can be seen by comparing the two expressions. If flux-profile relations are measured, this height is therefore the best height for the flux instrumentation.

Next we turn to the temporal and spatial scale in the fluctuations. As mentionned in section 2, they are best described in terms of spectra. Here we want to emphazise the aspect that:

$$\begin{aligned} \overline{x'^2} &= \int_{-\infty}^{\infty} S_1(k_1)dk_1 &&= \int_{-\infty}^{\infty} S(\omega)d\omega \\ \overline{u_j'x'} &= \int_{-\infty}^{\infty} Co_1(k_1)dk_1 &&= \int_{-\infty}^{\infty} Co(\omega)d\omega \end{aligned} \tag{14.81}$$

which states that the contribution to the variances and covariances from different wave-number or frequency scales are described by the spectra and the co-spectra. As discussed in section 2 the relation between the wave number and the frequency is given as a good approximation by Taylor's hyphotesis, equation Eq. 14.10. Note that the co-spectra between a velocity signal and another signal describes the turbulence flux in the direction of the velocity component as discussed in section 3.

In section 2 is shown how the inertial subrange of the spectra scales with the relevant dissipations. Since the dissipations can be described as universal nondimensional functions of the relevant parameters in the different scaling regimes, this leads to the idea to describe the spectra in terms of the scaling laws considered in section 4. As an example we take the velocity spectrum in Eq. 14.8. We now substitute the Monin-Obukhov similarity function $\phi_\epsilon(z/L) = \kappa z\epsilon/u_*^3$ from Eq. 14.51 to obtain:

$$kS_u(k) = a_u\epsilon^{2/3}k^{-2/3} = a_u u_*^2\phi_\epsilon(z/L)(kz)^{-2/3} \tag{14.82}$$

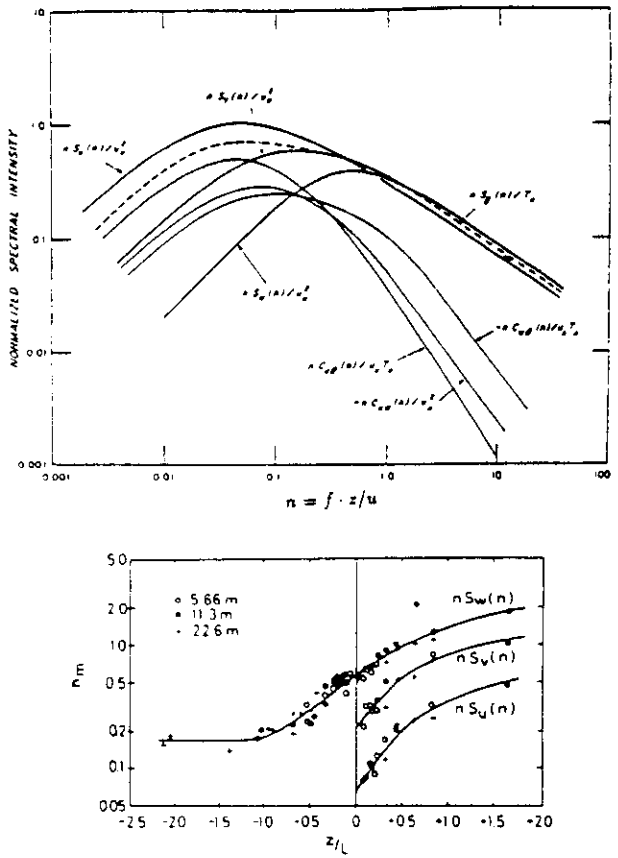

Figure 14.17: *Normalized surface-layer spectra for neutral conditions together with the variation of the peak frequency n_m with z/L for the vind spectra (Kaimal et al., 1972).*

Comparing with Eq. 14.10 we expect that after proper normalization, at least the inertial subrange forms of the spectra and co-spectra can be written as universal functions of z/L and a normalized frequency, n:

$$n = fz/u = k_1 z/2\pi = z/\lambda \tag{14.83}$$

where λ is the wave length corresponding to k_1.(NB. In micrometeorological literature, there has been a confusing change in notation. Earlier f was denoted n and vice versa).

One of the results of the Kansas experiment was that the relevant spectra could indeed be universally described over most of the frequency range according to Eqs. 14.82 and 14.83. From Kaimal et al. (1972) we present the important surface layer spectra.

Since all instruments or combinations of instruments can be characterized by a spatial and frequency resolution, the spectra in Figure 14.17 can be used to estimate the amount of variability that remains with a certain averaging time and how large a fraction of a given (co)variance a given sensor system can resolve. For example if one uses an averaging time, T, and a time resolutuion, t, one can resolve not the whole of $\overline{u_j'x'}$ in Eq. 14.81 but only $\overline{u_j'x_m'}$ given by:

$$\overline{u_j'x_m'} = 2\int_{2\pi/T}^{2\pi/t} \mathrm{co}(\omega)d\omega, \tag{14.84}$$

where we have used that co-spectra are even functions of frequency.

Since the publication of this Figure 14.17, Kaimal et al., (1976); Højstrup (1982) have documented that also the spectra in the mixed layer can be scaled with the relevant scales here to give universal forms. Furthermore, Sorbjan (1986) has shown that also when the local scaling apply, the spectra adapt to this form as well. In the unstable surface layer it has been shown that the eddies in the mixed layer give a footprint in the surface layer spectra, especially for horizontal velocity components and temperature. The result of this is that the peak of these spectra do not scale with z/L but rather with z_i (Højstrup, 1982). This was actually the reason for the absence of n_m plots for these spectra in Figure 14.17. The z/L formulation could not be brought to describe the data. Finally, Højstrup et al. (1990) have shown that also for neutral conditions the low frequency component of the velocity spectra scale with the boundary layer height, not only with the measuring height as implied by the surface layer scaling. Finally, Olesen et al. (1984); Larsen et al (1985, 1990) have demonstrated the importance of the gravity waves in the spectra for stable conditions. These yield spectral components that scale as:

$$kS(k) \sim N^2k^{-2} \tag{14.85}$$

where N is the Brunt-Vaisala frequency given by Eq. 14.72.

In Figure 14.18, we present examples of spectra of the horizontal velocity components in the surface layer, including the z_i-part for unstable conditions and the gravity wave part for stable conditions.

An important issue for all experimental work is the statistical confidence of the data and its relation to the choice of averaging time (or length if spatial data are available). We shall here refer to the discussion in Wyngaard (1973). Consider the variance of x around x_T where:

$$x_T(t) = \frac{1}{T}\int_{t-T/2}^{t+T/2} x(t+t')dt' \tag{14.86}$$

We can now compute the variance, δ_T^2 , as:

$$\delta_T^2 = \overline{(x(t)-x_T(t))^2} = 2\overline{x'^2}/T\int_0^T(1-t'/T)\rho_x(t')dt'$$

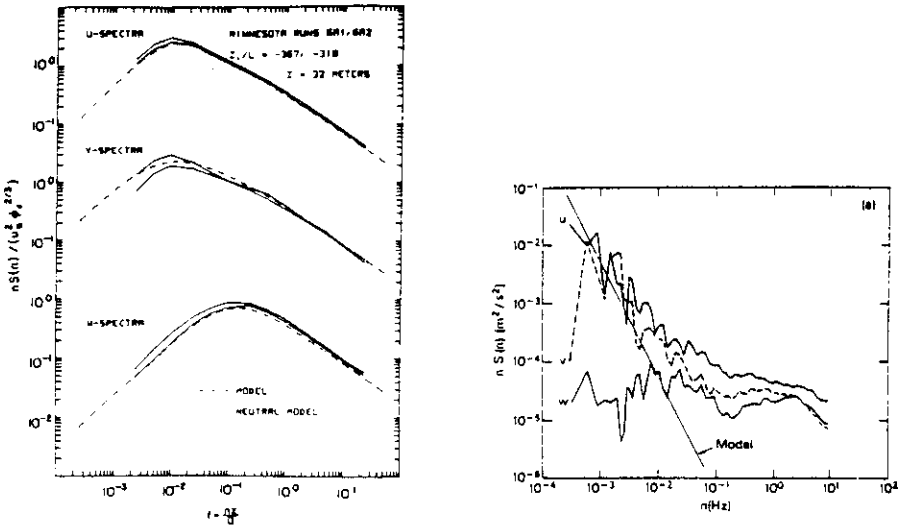

Figure 14.18: *Surface layer spectra for (a) unstable and (b) stable conditions, showing the influence of the mixed layer scaled eddies and the gravity waves, respectively (Højstrup, 1982; Larsen et al., 1985).*

where $\rho_x(t') = \overline{x(t)x(t+t')}/\overline{x'^2}$. We now assume that T is large enough for the integral to become equal to the integral of the correlation function.

With the approximation cited above, we can write as:

$$\delta_T^2 = 2\overline{x'^2}\tau/T \tag{14.87}$$

If the accuracy to be achieved is written as $a^2 = \delta_T^2/\bar{x}^2$, we can finally reverse Eq. 14.87 to give the averaging time, T_a, to achieve the relative accuracy of a^2

$$T_a = 2\frac{\tau_x}{a^2}\frac{\overline{x'^2}}{\bar{x}^2} \tag{14.88}$$

In Eq. 14.88 the integral scale, τ_x, that can be estimated by the peak frequency for the spectra presented in figures 7.1 and 7.2 will vary roughly between $z/\bar{u}$ and $h/\bar{u}$ for unstable conditions and somewhere between $z/\bar{u}$ and $L/\bar{u}$ for stable conditions, varying from signal to signal. To estimate the mean speed for example, equation Eq. 14.88 takes the form:

$$T_{a,u} = \frac{2\tau_u}{a^2}\frac{\overline{u'^2}}{\bar{u}^2} \tag{14.89}$$

For the surface layer we take $\tau_u = z/\bar{u}$ and $\overline{u'^2}/\bar{u}^2$ the turbulence intensity as 0.05. We then find that at $z = 5$ m we can achieve for $u = 5$ m/s a 1 per cent accuracy for 15 min averages.

To estimate the necessary averaging time for the variances and covariances, one must substitute these quantities for x to obtain e.g.:

$$\overline{u'^2} : \overline{x'^2}/\bar{x}^2 = \overline{(u'^2 - \overline{u'^2})^2}/(\overline{u'^2})^2 = \overline{u'^4}/(\overline{u'^2})^2 - 1$$

Correspondingly for a covariance:

$$\overline{w'y'} : \bar{x}'^2/\bar{x}^2 = \overline{w'y'^2}/(\overline{w'y'})^2 - 1$$

For the variances the result is seen to be the flatness factor. Since even order moments of turbulence are not too far from Gaussian, the flatness factor has a value of about 3. For the variances we therefore find :

$$T_{a,x^2} = 4\,\frac{\tau_x}{a^2} \tag{14.90}$$

By comparing with Eq. 14.89 this is seen to be of the order $\frac{a^2}{u'^2} = 20$-100 times larger than averaging time necessary to obtain the average wind speed for the same accuracy a provided the integral scale is the same for the two processes which is a reasonable assumption. It therefore seems inescapable that estimating the standard deviations with 1 per cent is out of question in the real world where the stationarity of the turbulence over periods more than a few hours is questionable. Based on data for the different moments obtained from the Kansas experiments, Wyngaard (1973) furthermore concludes that for the same accuracy the necessary averaging time for the covariances is between 3 and 20 times the averaging time for the variances. This makes it necessary to reduce the demands to the accuracy for the covariances even further than for the variances.

Furthermore, one can study the demands to averaging time for moments of higher order than the variances and covariances discussed above. One finds that it becomes almost impossible to determine these higher-order moments in the atmosphere because the averaging time must be limited to time periods substantially less than the diurnal cycle to avoid the problems with instationarity.

Finally, we shall consider the instrumentation problems. Overall the well-known instruments of today are both accurate and reliable. Most of the problems encountered, therefore, are not fundamental measuring technological problems, but are more associated with that the experimentator forget to assure himself about certain uncertainties. For velocity measurements calibration and flow distortion remain important problems. Especially for anemometers with empirical calibrations like cup anemometers, careful periodic calibrations must be recommended. Also flow distortion has been found to be important for velocity measurements and several models for flow distortion have now been developed. Flow distortion originates from the instruments themselves or from the platforms, and even very slender booms have been shown to give rise to surprisingly large flow distortion. Generally two different ways of handling flow distortion effects are used. One method consists in

comprehensive wind tunnel calibrations, that ideally allow to compute a *time* velocity vector for each measured value of the same vector. This method is e.g. illustrated in Mortensen et al. (1987).

The other method involves estimating the effects on mean values and turbulence statistics, using more or less sophisticated models for the physics of the flow distortion. These models are subsequently reversed to yield *time* mean values and turbulence statistics from the measured values. The simplest *model* is here just tp rotate the coordinate system along the measured mean flow (Dyer, 1981, 1982, Wyngaard, 1982). More refined descriptions have been developed by Wyngaard (1981) for situations, where the distorting body is mauch smaller than the scale of turbulence, as is mostly the case for over land measurements in the surface layer. For scalar fluxes the flow distortion is less important generally than for velocity (Wyngaard, 1988). For temperature sensors, the dominating sneaky problem is the radiation errors, meaning that the temperature of the sensor is influenced by the radiation balance with the surroundings. Most temperature sensors need calibration, so the need to calibrate should not be a surprise, but the radiation errors might even for a well screened sensor influence the measurements systematically through some unsuspected heat bridge in the system without showing dramatic and easily detectable errors. Humidity sensors are a larger problem because both for mean value and turbulence measurements the humidity sensors are more complicated and/or less accurate than the temperature and velocity sensors. Here is really a need for sensor development. Finally should be mentioned the contamination problem with salt, a problem that of course is largest over the ocean or in the coastal region. Due to the hygroscopic qualities of salt, salt contamination can be totally destructive to the data quality of both temperature and humidity measurements. There is presently no solution to this problem aside from repeated cleaning of the sensors.

14.8 Uncertainties and unknowns for the simple PBLs

Many of the uncertainties for the simple planetary boundary layers are associated with the assumptions behind the descriptions not being sufficiently fulfilled in the real world. The models describing the total boundary layer are accepted to be more uncertain than the surface layer descriptions, and we shall defer much of the discussion about the total boundary layers to the next section that concerns inhomogenous situations.

If one looks closer on the assumptions for a surface layer, one sees that it demands that $z_0 << z << h$ (Tennekes, 1973 and 1982). As is obvious, these constrains are not always fulfilled. Therefore, one should not be too surprised to find deviations from the pure surface layer theory in the measurements. Close to very rough surfaces, as over cities and forests, the deviations from the simple surface layer ϕ functions are generally found (Garratt, 1978; Raupach, 1979). Also, if the unequality above is not well fulfilled one should expect to see processes scaling with z_0 or h show up in the surface layer. In section 7 we have already seen that h becomes an important scale for describing the spectra in what is otherwise considered the surface layer. This fact of course must have consequences for other quantities as well. Indeed, analyses of surface layer data including the pressure part of the flux divergence terms of Eq. 14.51 conclude (Elliot, 1972; McBean and Elliot, 1975) that the flux divergence term s does not scale with z/L alone as assumed in Eqs. 14.51 and 14.52. This means that one should not be surprised that some authors find some differences for the terms in these equations.

In the surface layer formalism, the von Kármán constant is an universal constant because in the analysis it cannot depend on anything. If we relax the strict surface layer formulation, then it may depend on parameters like z_0 and h. Indeed, in recent measurements variations variation of κ with the roughness Reynolds number, see Fig. 14.19.

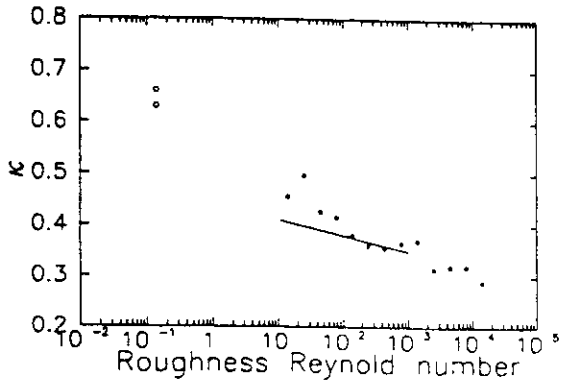

Figure 14.19: *Recent data on the variation of the von Kármán constant with roughness Reynolds number, according to Oncley et al. (1990), —, Mortensen et al. (1987), •, and Gryning (1993), △. The values shown are averages over extensive data sets*

For a large fraction of the stable boundary layer situations one encounters in practice thaat the Richardson number is larger than the critical Ri, simultaneously with that vertical transport still take place through intermittently occuring turbulence, see section 4. Various ad hoc formulations have been proposed e.g. by modellers that have noticed that if they use standard flux parameterization schemes, their stable boundary layers collapse much faster and more often than the data show (Estournel and Guedalia, 1987). However, a consistent theory still has to be formulated.

Overlapping the above, the stable boundary layer is known to include different kinds of wave activities that are not systematically described, but which have at least been shown to contribute to the velocity spectra in a describable systematic way. Also the stable boundary layer is the boundary layer where the h/z_0 ratio in general is smallest because h tends to be small. Therefore the concept of surface layer might get into difficulties here before into n any other conditions. Undoubtedly, the future will see progress within this area, so that last often occurring boundary layer phenomena can be included in the list of processes, we understand.

14.9 Horizontally inhomogeneous boundary layers

After having discussed the stationary and horizontally homogeneous boundary layers, that are easy to define and almost non-existing, we turn towards the horizontally inhomogeneous boundary layers, that are everywhere, but almost impossible to specify because they come in so many versions.

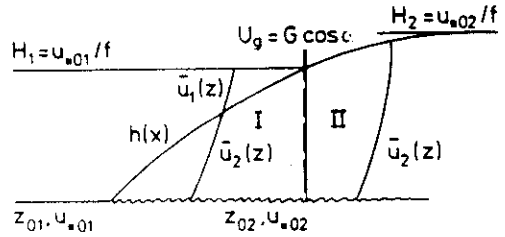

Figure 14.20: *Growth of an internal boundary layer from a smooth to rough transition under neutral conditions. Eventually the internal boundary layer height, $h(x)$ grows to establish a new boundary layer (Sempreviva et al., 1990).*

Normally one distinguishes between the effects of changes in terrain elevation and changes in surface characteristics like z_0, z_{0T} and z_{0q}, q_0 and θ_0. This is because the former influences the flow through the pressure term, while changes in surface characteristics diffuse up into the boundary layer by the turbulent diffusion.

Basically two different methods exist for handling inhomogeneous surface characteristics, when trying to estimate the flux between the atmosphere and an inhomogeneous area. In one method the inhomogeneous surface is broken down into a number of destinct subareas, that are each considered homogeneous, and with step changes in the surface characteristics in between. In the other method one estimates area averages of the surface characteristics $z_0, z_{0T}, z_{0q}, \theta_0$ and q_0 by a suitable average across the inhomogeneous terrain in question.

Considering the first approach first, we concentrate for starters on a step change in roughness, and start with neutral stability. A simple but accurate way of estimating the effect of this is to assume that the information about the surface change propagate upwards with u_*, leading to the following expression for the growth of an internal boundary layer, $h(x)$ with fetch, x, over the new surface:

$$dh/dx = au_*/u(h) \tag{14.91}$$

where a is a constant of order one. Eventually h will grow untill it fill out the boundary layer, and a new boundary layer is established. The idea is presented in Figure 14.20.

Integration of Eq. 14.91 yields:

$$cx/z_0 - 1 = (\ln(h/z_0) - 1)h/z_0 \tag{14.92}$$

where c is another constant of order unity. Equation 14.92 is seen to describe a growth of the internal boundary layer that is slightly slower that x to the power of one. To get the change in surface stress one matches the upstream and downstream velocity profiles in the $h(x)$ to obtain:

$$u_{*2}/u_{*1} = \ln(h(x)/z_{01})/\ln(h(x)/z_{02}) = 1 + \frac{\ln(z_{02}/z_{01})}{\ln h/z_{02}} \qquad (14.93)$$

This equation is found to describe data very well and to works even better than second- order closure models (Larsen et al., 1982). It is seen to describe a variation with x that is strongest in the beginning when h is small, followed by a very slow change when h has become large. From Eq. 14.93 the ratio between the wind speeds are found to be:

$$\bar{u}_2(z)/\bar{u}_1(z) = \frac{u_{*2}}{u_{*1}} \ln(z/z_{02})/\ln(z/z_{01}) \qquad (14.94)$$

which is seen to vary less than the u_*-ratio because the two z_0's enter oppositely in Eq. 14.94 than in Eq. 14.93. Sempreviva et al. (1990) have modified the profile formulations in Eq. 14.94 and extended the formulation to include the effect of a final boundary layer height. Jensen et al., (1984) have extended it to non-neutral cases showing that the growth rate of the internal boundary varies between $x^{1/2}$ and $x^{3/2}$ times, dependent on stability conditions a[illegible]ght of $h(x)$. Note that the equation for the growth of an unstable boundary layer Eq. 14.75 can be used for the growth of an internal boundary layer, interpreting t as $x/\bar{u}$. The second-order modeling of Rao (1974) and Rao et al. (1974, 1974a) argely confirms the content of the above equations. The studies of Sempreviva et al. (1990) seem to indicate that it takes the surface wind speed a fetch of about 10 km before it has fully adapted to the new surface. The stability extension of the model Eq. 14.91 through Eq. 14.93 by Jensen et al. is simplistic in the sense that the same stability is assumed for both areas. There have never been tested a model system of this type that includes changes in all the surface characteristics, $z_0, z_{0T}, z_{0q}, \theta_0$ and q_0, θ_* and q_* simultaneously. The difficulties shall not be underestimated, although the roughnesses can probably be related, as described in section 14.6. Also some of the difficulties are probably not associated with the model concepts, but more associated with keeping track on the many and different subsurfaces with each their characteristics.

The direct area averaging of the surface characteristics of an inhomogeneous area sounds simpler than the approach cited above. Taylor (1987) suggests as a practical formula to average the z_0 values:

$$\ln(z_{0a}) = \int_A \ln(z_0(x))dx \qquad (14.95)$$

where the x-integration is carried out over the area in question to obtain the effective z_{0e}. To use this type of averaging of surface characteristics, it is important to know its meaning. We can write the area averaged profile equations, from Wood and Mason (1991),corresponding to Eq. 14.61 with d neglected for simplicity:

$$\begin{aligned} < u(z) > &= \frac{(< u_*^2 >)^{1/2}}{\kappa}\left(\ln(z/z_{oe}) - \psi_m(\frac{z}{L_e})\right) \\ < \theta(z) > - < \theta_0 > &= \frac{< -\overline{w'\theta'} >}{\kappa(< u_*^2 >)^{1/2}}\left(\ln(\frac{z}{z_{0Te}}) - \psi_h(\frac{z}{L_e})\right) \end{aligned} \qquad (14.96)$$

where we use <> as area average and try to relate the area averaged surface fluxes to the area averaged mean values,with the zoe value being determined such that Eq. 14.96 is true. L_e is the corresponding Monin-Obukhov length. A concept used much in these considerations is the blending height, l, a height above w[illegible] the mean values has been blended enough not to vary across the inhomogenous area. The stress on the other hand is supposed still to vary. This difference between the mean values and the stress, was seen as well in connection with the step change model Eqs. 14.93 and 14.94. Using the blending height concept one can now derive corrections to Eq. 14.95. Different authors use different blending heights. Wieringa (1976) and Claussen (1991) prefer a height related to the height of the roughness element, while Mason (1988) and Wood and Mason (1991) prefer a height related to the horizontal scale for the roughness changes, and the same upward diffusion rate, use in the step change model. Mason (1988) and Wood and Mason (1991) derives estimates of z_{0e} and z_{0T_e} to find that z_{0e} tend to be larger than z_{0a}, while z_{0T_e} tend to be smaller than z_{0T_a}. However it must be emphazised that the z_{0e} values thus estimated are quite strongly dependent on which of the parameters in Eq. 14.96 one considers measured, and which one wants to estimate. They have thus become somewhat removed from the physical definition of a roughness length, and become more like a sub-grid scale process outputting some area averaged parameters, when others are inserted in the formal profile equations Eq. 14.96. The fact that the atmosphere feels a surface change through a diffusion process as depicted by Eq. 14.93 can be used when interpreting real data into a framework of the homogeneous models, considered in section 4 through 7. The simplistic way of phrasing the models of internal boundary layers (IBL) after a step change is to say that the IBL growth as between x/10 and x/200 dependent on which arameter one uses to characterise the IBL. This can be turned two ways. If one measures from a mast at height z, it means that surface changes closer than 10z, can not be seen in the data. If on the other hand, one wants to use the resistance laws in section 6 with a characteristic roughness together with the wind at z = 1km, it means that this roughness must be characteristic for an area with a width between 10 and 200 km. Next we turn to the effects of changing surface elevation. The recent advances here start with a study by Jackson and Hunt (1975) who studied the turbulent flow over a two dimensional low ridge. The result are illustrated on Figure 14.21.

The result of Jackson and Hunt (1975) and the later research (e.g. Zeman and Jensen, 1987) was that the pressure field was perturbed out to a distance of L, and the inner height, l, was the level with the maximum speed perturbation. Below l the stress achieved equilibrium with the new shear and speed ℓ was related to L through an equation similar to Eq. 14.93: $\ell \ln(l/z_0) \sim L$.

Later the results of Jackson and Hunt (1975) was combined with a linearized flow model, where the scale L was replaced by the the wave length of the Fourier decomposition (Troen and Petersen, 1989). From Eq. 14.32 the linearized equations of motion for neutral stationary flow perturbations can be written:

$$U_0 \frac{\partial u_i}{\partial x_j} = \frac{1}{\rho}\frac{\partial p}{\partial x_i} + \frac{\partial}{\partial z}\tau \qquad (14.97)$$

where subscript 0 indicates background flow, and where only the important terms have been retained. The kinematic boundary equations at the surface $z = H(x, y)$ are given by:

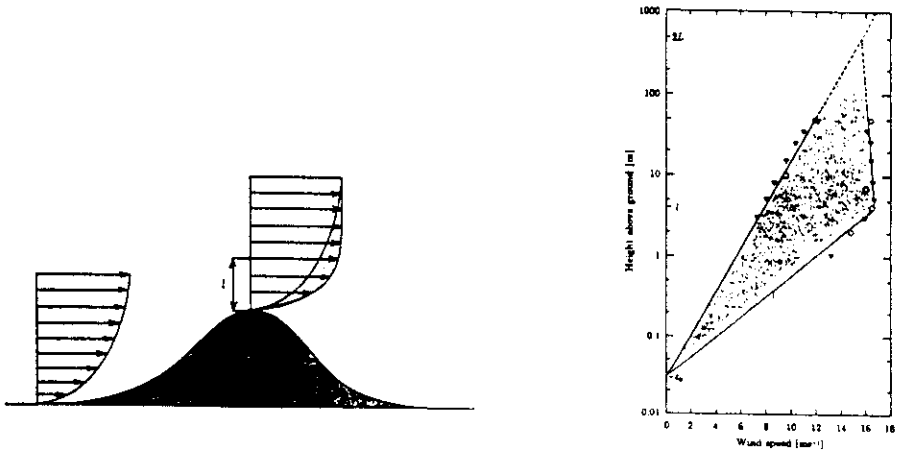

Figure 14.21: *a) Characteristic of the flow over a two dimensional low ridge according to Jackson and Hunt (1975), taken from Troen and Petersen (1989). The scale of the hill, L, and the socalled inner scale, ℓ, is shown. b) Experimental data from Jensen et al. (1984).*

$$w = \mathbf{u_0} \cdot \Delta H(x, y) \tag{14.98}$$

The equations Eqs. 14.97 and 14.98 are well suited for solution through the two dimensional Fourier transform in the coordinates horizontal coordinates. To connect to the Jackson-Hunt theory the hill scale, L , of Figure 14.21 is related to wavenumber, i.e. $L \sim |k|^{-1}$. With this relation the Jackson-Hunt model can now be used to close the vertical parts of the equation. The association of the scale L with a reciprocal wave number is neat, but it does not necessary work. Fortunately extensive test of the models again available data and models show it to work remakably well (Walmsley et al,1990). In their program for evaluating the wind potential of a given site Troen and Petersen (1989) managed to combine a roughness change model of the step change type Eq. 14.91 through Eq. 14.94 with an orographic model, just described, and a sheltering model, not described here. Aside from meteorological data from a neighbouring station, the users input to the program is three maps, one showing the location and types of shelters, one showing the terrain elevations, and one showing the distribution of roughnesses, We illustrate here the last with a roughness map.

The idea of using Fourier transforms of terrain elevation has by Belcher et al (1990) been extended to the roughness change study, Fourier transforming $\ln(z_{01}/z_{02})$, compare Eq. 14.93, from roughness maps like Figure 14.22. This is combined with an analysis of the flow perturbation adapter from the hill studies by Jackson and Hunt (1975). An attractive aspect of this Fourier transform approach is that it could be extended to three dimensions fairly easily, thereby faciliating computation of area averaged flow fields and fluxes much more than the more rigidly two dimensional formulations in Eq. 14.91 through Eq. 14.94.

It is instructive to compare the maps necessary for the wind energy evaluation with the corresponding needs if the goal was to compute the fluxes of momentum, heat and moisture from the same area.

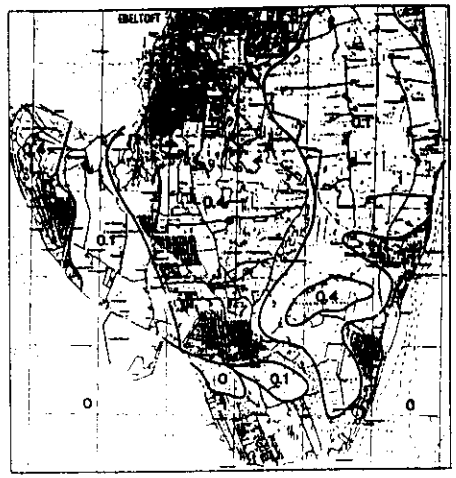

Figure 14.22: *The figure illustrate an input map with roughnesses to the analysis program for wind energy potential(Mortensen et al,1992)*

Here we would also need the orography map, and the roughness map. Probably we would not need the map of sheltering effects. Additionally we would need maps over θ_0 and q_0, z_{0T}, and z_{0_q} could probably be related to z_0, as discussed in section 5. The major model modification would be, that while the wind energy model works satisfactorily as a neutral model, because the main interest is on reasonable high winds,then a model describing the fluxes would necessarily have to be be able to describe non neutral flows as well. The model should be able to handle quite extreme thermal conditions. Extremes in thermally controlled situations are found ind the arctic both associated with the polynia research and in the marginal ice zone, where the temperature difference between the water and the ice surfaces can be tens of degrees (Andreas, 1980, Claussen, 1991).

However, also in more temperate climates, large changes in surface temperature and humidity as well the associated fluxes take place on the border between land and water, so also here non neutral models become essential. In the stable boundary layer, a description is complicated by that even moderate stability and moderate terrain variation can set up thermally controlled local flow (Mahrt and Larsen, 1990). Of these effects the non-homogeneous stable boundary layers are probably most difficult to handle, because of the weak vertical fluxes. This, on the other hand may be less important, when the overall objective of the PBL study as here is to estimate the vertical fluxes. The strongly thermally driven internal boundary layers offer little problems, precisely because of the strong vertical fluxes. They can be described the same way as a growing strongly unstable boundary layer, substituting $x/\bar{u}$ for t.

The discussion above has been concentrated on the response of the boundary layer to inhomogeneous surface conditions. As a note of caution it should therefore be pointed out that inhomogeneity in the boundary layer might be due to other reasons as well. E.g. slowly developing synoptic systems and cloud systems will influence inhomogeneity that originally is independent of the surface conditions,

although the surface might be influenced by for example clouds changing the radiation conditions at the surface.

Finally we should mention the studies spectra in inhomogeneous terrain, basically the low frequency part of the spectra increase for complex terrain, a fact that as least qualitatively can be associated with the contributions of the terrain variations to a larger scale roughness (Panofsky et al. 1982). In studies of spectrum response to step changes in roughness and heatflux Højstrup (1981) and Højstrup et al. (1982) describes how the inertial subrange of the spectra adjust to balance with the local stress as in Eq. 14.82, while the lower frequency parts have a larger memory, and more slowly relaxes towards the new boundary layer conditions.

14.10 Discussion and conclusion

In conclusion to this presentation, I should like to point out, that while I have discussed many aspects of the planetary boundary layer, I have not presented any recommendations for which type of description to use to describe the different processes. This is partly to save place in an already long paper, but also because I believe, that given the uncertainties on the the different descriptions, the reader will have make the choise between different and competing methods, parameters etc him/her self. In a qualitative sense most of the acknowleged methods and parameter choises are equaly good, and to prodceed deeper, one will have to dive into the litterature anyhow. I have therefore only tried to refer to papers and books, where the different expressions are summarized, while here concentrating on a general description on the current knowledge about the prosesses and parameters of importance. Finally, I hope that I have conveyed the impression of the importance of the simple ideas in turbulence closures, namely all closure is closure based on K-diffusivity and the smaller the scale of closure the more general the results.

Acknowledgement.

I wish to acknowledge inspiration and discussions with students and teachers during the meeting of the Study Institute in Glücksburg. Also thanks are due to my colleagues at Risø for support, notably Niels Otto Jensen who patiently participated in many clarifying discussions. Last but not least I wish to thank Birthe Skrumsager for her efforts with shaping up the output of my wordprocessor in all too little time.

14.11 References

Andreas EL (1980) Estimation of heat and mass fluxes over arctic leads. *Mon Wea Rev* 108: 2057-2063.

Araya SPS (1973) Contribution of form drag on pressure ridges to the air stress on arctic ice. *J Geophys Res* 78: 7092-7099.

Araya SPS (1978) Comparative effects of stability, baroclinity and the scale-height ratio on drag laws for the atmospheric boundary layer. *J Atmos Sci* 35: 40-46.

Arpaci VS, Larsen PS (1984) Convection heat transfer. *Prentice-Hall* 512pp.

Belcher SE, Xu DP, Hunt JCR (1990) The response of a turbulent boundary layer to arbitrarily distributed two-dimensional roughness changes. *Quart J Roy Met Soc* 116: 611-635.

Berkowicz R, Prahm LP (1979) Generalization of K-theory for turbulent diffusion. Part1: Spectral turbulent diffusivity concept. *J Appl Meteor* 18: 266-272.

Brown RA (1980) Longitudinal instabilities and secondary flows in the planetary boundary layer: a review. *Rev Geophys Space Phys* 18: 683-697.

Brutsaert WH (1975) Comments on surface roughness parameters and the height of dense vegetation. *J Met Soc Japan* 53: 96-97.

Brutsaert WH (1982) Exchange processes at the earth atmosphere interface. In: **Engineering** Meteorology (Ed. E. Plate) *Elsevier* 319-369.

Busch NE (1973) On the mechanics of atmospheric turbulence. In: Workshop on Micrometeorology. (Ed. D.A. Haugen). *Am Met Soc* Boston, Mass., 1-28.

Busch NE (1975) Fluxes in the surface boundary layer over the sea. In: Modelling and prediction of the upper layers of the ocean *NATO ASI* Ed.: E.B. Kraus 72-91.

Busch NE, Larsen SE, Thomson DW (1979) Data analysis of atmospheric measurements. *Proc Dyn Flow Conf 1978* (Eds E.G.K. Kovasznay et al.) Dantec, Skovlunde, Denmark, 887-908.

Businger JA, Wyngaard JC, Izumi Y, Bradley EF (1971) Flux-profile relationships at the atmospheric surface layer. *J Atmos Sci* 28: 191-189.

Businger JA, Araya SPS (1974) Height of the mixed layer in the stably stratified planetary boundary layer. *J Atmos Sci* 18: 181-189.

Businger JA (1982) Equations and concepts.In: Atmospheric Turbulence and Air Pollution Modelling. Eds.: F.T.M. Nieuwstadt and H. van Dop. *Reidel* Dordrecht, Holland. 1-36.

Caughey SJ (1982) Observed characteristics of the atmospheric boundary layer. In: **Atmospheric** Turbulence and Air Pollution Modelling (Edss. F.T.M. Nieuwstadt and H. van Dop) *Reidel Holland* 107-158.

Chapman S, Cowling TG (1970) The mathematical theory of non-uniform gases. *Cambridge University Press* Cambridge, 422 pp.

Charnock H (1955) Wind stress on a water surface. *Quart J Roy Met Soc* 81: 639-640.

Clarke RH, Hess GD (1973) On the appropriate scaling for velocity and temperature in the planetary boundary layer. *J Atmos Sci* 30: 1346-1353.

Claussen M (1991) Local advection processes in the surface layer of the marginal ice zone boundary layer. *Bound Lay Met* 30: 327-341.

Courtney M, Troen I (1990) Wind speed spectrum from one year of continuous 8 *Hz* measurements. *Proc Ninth Symp Turbulence and Diffusion* (AMS, Boston, USA), 301-304.

Deardorff JW (1970) Convective velocity and temperature scales for the unstable planetary boundary layer and for Rayleigh convection. *J Atmos Sci* 27: 1211-1213.

Deardorff JW (1972) Parameterization of the planetary boundary layer for use in general circulation models. *Mon Wea Rev* 100: 93-100.

Delage Y (1988) A parameterization of the stable atmospheric boundary layer. *Bound Lay Met* 43: 365-381.

Dyer AJ (1974) A review of flux-profile relationships. *Bound Lay Met* 7: 363-372.

Dyer AJ (1981) Flow distortion by supporting structures *Bound Lay Met* 20: 243-251.

Dyer AJ (1982) Reply (to comment by J.C. Wyngaard). *Bound Lay Met* 22: 267-268.

Ekman VW (1905) On the influence of the earth rotation on ocean currents. *Arkiv, Math Astron O Fysik* 2: 11.

Elliott JA (1972) Microscale pressure fluctuations measured within the lower atmospheric boundary layer. *J Fluid Mech* 53: 351-383.

Estournel C, Guedalia D (1987) A new parameterization of eddy diffusivities for nocturnal boundary layer modelling. *Bound Lay Met* 39: 191-302.

Fairall CW (1987) A top-down and bottom-up diffusion model of CT_2 and Cq_2 in the entraining convective boundary layer. *J Atmos Sci* 6: 1010-1017.

Garratt JR (1978) Flux profile relations above tall vegetation. *Quart J Roy Met Soc* 104: 199-211.

Gryning SE, Batchvarova E (1990) Analytical model for the growth of the coastal internal boundary layer during onshore flow. *Quart J Roy Met Soc* 116: 187-203.

Gryning SE (1993) Meteorological measurements over Kattegat. Marine Research Program 90 Report. National Agency of Environmental Protection in Denmark, Copenhagen, Denmark.

Hasse L (1976) A resistance-law hyphothesis for the nonstationary advective planetary boundary layer. *Bound Lay Met* 10: 393-407.

Hill RJ (1989) Implications of Mounin-Obukhov similarity theory for scalar quantities. *J Atmos Sci* 46: 2236-2244.

Holtslag AAM, Nieuwstadt FTM (1986) Scaling in the atmospheric boundary layer. *Bound Lay Meteorol* 36: 201-209.

Högström U 1990: Analysis of turbulence structure in the surface layer with a modified similarity formulation for near neutral conditions. *J Atmos Sci* 47: 1949-1972.

Højstrup J (1981) A simple model for adjustment of velocity spectra in unstable conditions downstream an abrupt change in surface roughness and heat flux. *Bound Lay Met* 21: 341-356.

Højstrup J (1982) Velocity spectra in the unstable planetary boundary layer. *J Atmos Sci* 39: 2239-2248.

Højstrup J,. Larsen SE, Jensen NO (1982) Results from an experimental investigation of a step change in surface heat flux. Proceedings of First International conference on Meteorology andd Air-Sea Interaction of the Coastal Zone. *Amer Met Soc* Boston, US, 28-30.

Højstrup J, Larsen SE, Madsen PH (1990) Power spectra of horizontal wind components in the neutral atmospheric surface boundary layer. In: *Ninth Symp turbulence and diffusion* (AMS, Boston, USA), 305-308.

Jackson PS, Hunt JRC (1975) Turbulent wind flow over a low hill. *Quart J Roy Met Soc* 101: 929-955.

Jackson PS (1981) On the displacement height in the logarithmic velocity profile. *J Fluid Mech* 111: 15-25.

Jensen NO, Petersen EL, Troen I (1984) Extrapolation of mean wind statistics with special regard to wind energy application. WCP-86. *WMO*

Jensen NO (1991) Comments on surface parameterization. In: WMO Planetary Boundary Layer Model Evaluation Workshop, August, 1989, Reading UK. Ed.: J.C. Wyngaard, *WMO/TD-No. 378* 40-42.

Kaimal JC, Wyngaard JC, Izumi Y, Coté OR (1972) Spectral characteristics of surface-layer turbulence. *Quart J Roy Met Soc* 1972: 563-589.

Kaimal JC, Wyngaard JC, Haugen DA, Coté OR, Caughey SJ, Readings CJ (1976) Turbulence structure in the convective boundary layer. *J Atmos Sci* 33: 2152-2169.

Larsen SE, Hedegaard K, Troen I (1982) Change of terrain roughness problem extended to mesoscale fetches. First International conference on meteorology and air/sea interaction. *Am Met Soc* Boston, USA. 8-13.

Larsen SE, Olesen HR, Højstrup J (1985) Parameterization of the low frequency part of spectra of horizontal velocity components in the stable surface boundary layer. In: Turbulence and Diffusion in Stable Environments. (Ed. J.C.R. Hunt), *Clarendon* Oxford, UK, 181-204.

Larsen SE, Courtney M, Mahrt L (1990) Low frequency behaviour of horizontal velocity spectra in stable surface layers. In: Ninth Symposium on turbulence and diffusion, *Am Met Soc* Boston, USA. 401-404.

Lettau H (1969) Note on aerodynamic roughness-parameter estimation on the basis of roughness-element distribution. *J Appl Met* 8: 828-832.

Lumley JL, Panofsky HA (1964) The structure of atmospheric turbulence. *Interscience* New York, 239 pp.

Mahrt L (1985) The vertical structure and turbulence in the very stable boundary layer. *J Atmos Sci* 42: 2333-2349.

Mahrt L 1986: On the shallow motion approximations. *J Atmos Sci* 43: 1036-1044.

Mahrt L, Larsen S (1990) Relation of slope winds to ambient flow over gentle terrain. *Bound Lay Met* 53: 93-102.

Mason PJ (1988) The formation of areally-averaged roughness lengths. *Quart J Roy Met Soc* 114: 399-420.

McBean GA, Elliott JA (1975) The vertical transport of kinetic energy by turbulence and pressure in the boundary layer. *J Atmos Sci* 32: 753-766.

Melgargo JW, Deardorff JW (1974) Stability functions for the boundary-layer resistance laws based on observed boundary layer heights. *J Atmos Sci* 31: 1324-1333

Mizuno T, Panofsky HA (1974) The validity of Taylor's hypothesis in the atmospheric surface layer. *Bound Lay Met* 9: 375-380

Mortensen NG, Larsen SE, Troen I, Mikkelsen T (1987) Two-years-worth of turbulence data recorded by a sonic-anemometer-based data aquisition system. Sixth Symposium on Meteorology and Instrumentation. *Am Met Soc* Boston, USA, 393-396.

Mortensen NG, Landberg L, Troen I, Petersen EL (1992) Wind atlas analysis and application program(WAsP). User's Guide. ISBN 87-550-1789-4. *Risø National Laboratory* Roskilde, Denmark, 130pp.

Nicholls S, Readings GJ (1979) Aircraft observations of the structure of the lower boundary layer over the sea. *Quart J Roy Met Soc* 105: 785-802

Nieuwstadt FTM (1984) The structure of the stable nocturnal boundary layer. *J Atmos Sci* 41: 2202-2216.

Obukhov AM (1971) Turbulence in an atmosphere with non-uniform temperature. *Bound Lay Met* 2: 7-29.

Olsen HR, Larsen SE, Højstrup J (1984) Modelling velocity spectra in the lower part of the planetary boundary layer. *Bound Lay Met* 29: 285-312.

Oncley SP, Businger JA, Friehe CA, LaRue JC, Itsweire EC, Chang SS (1990) Surface layer profiles and turbulence measurements over uniform land under neutral conditions. In: *Ninth Symposium on Turbulence and Diffusion* (AMS, Boston, USA), 235-240.

Panofsky HA, Larko D, Lipschutz RC, Stone G, Bradley FF, Bowen AJ, Højstrup J (1982) Spectra of velocity components over complex terrain. *Quart J Roy Met Soc* 108: 215-230.

Panofsky HA, Dutton JA (1983) Atmospheric Turbulence. *John Wiley*

Pollard RT, Rhines PB, THOMSON RORY (1972) The deepening of the wind mixed layer. *Geophys Fluid Dynam* 4: 297-304.

Powell DC, Elderkin CE (1974) An investigation of the application of Taylor's hypothesis to the atmospheric boundary layer turbulence. *J Atmos Sci* 31: 990-1002.

Rao KS, Wyngaard JC, Coté OR (1974) The structure of two-dimensional internal boundary layers over a sudden change of surface roughness. *J Atmos Sci* 31: 738-746.

Rao KS, Wyngaard JC, Coté OR (1974a) Local advection of momentum, heat, and moisture in micrometeorology. *Bound Lay Met* 7: 331-348.

Raupach MR (1979) Anomalies in flux-gradient relationships over forest. *Bound Lay Met* 16: 467-486.

Sempreviva AM, Larsen SE, Mortensen NG, Troen I (1989) Response of neutral boundary layers to changes of roughness. *Bound Lay Met* 50: 205-225.

Sorbjan Z (1986) Local similarity of spectral and cospectral characteristics in the stable continuous boundary layer. *Bound Lay Met* 35: 257-275.

Stull RB (1988) An introduction to boundary layer meteorology. *Kluwer Academic Publishers* 666pp.

Taylor PA (1987) Comments and further analysis on the effective roughness lenth for use in numerical three-dimensional models. *Bound Lay Met* 39: 402-419.

Tennekes H (1973) The logarithmic wind profile. *J Atmos Sci* 30: 234-238.

Tennekes H, Driedonks AGM (1980) Basic entrainment equations for the atmospheric boundary layer. *Bound Lay Met* 20: 515-531.

Tennekes H (1982) Similarity relations, scaling laws and spectral dynamics. In: Atmospheric Turbulence and Air Pollution Modelling. Eds. F.T.M. Nieuwstadt and H. van Dop. *Reidel* Holland. 37-68.

Tennekes H, Lumley JL (1982) A first course in turbulence. *MIT Press* Cambridge MA, 300 pp.

Thom AS (1971) Momentum absorption by vegetation. *Quart J Roy Met Soc* 97: 414-428.

Troen I, Mikkelsen T, Larsen SE (1980) Note on spectral diffusivity theory. *J Appl Meteor* 19: 609-615.

Troen I, Petersen EL (1989) European Wind Atlas. *Risø National Laboratory* Roskilde. Denmark.

Walmsley JL, Troen I, Lalas DP, Mason PJ (1990) Surface layer flow in complex terrain: Comparison of models and full-scale observations. *Bound Lay Met* 52: 259-289.

Wieringa J (1976) An objective exposure correction method for average wind speeds measured at a sheltered location. *Quart J Roy Met Soc* 102: 867-889.

Wood N, Mason P (1991) The influence of static stability on the effective roughness length for momentum and heat transfer. *Quart J Roy Met Soc* 117: 1025-1056.

Wyngaard JC, Coté OR (1971) Cospectral similarity in the atmospheric surface layer. *Quart J Roy Met Soc* 98: 590-603.

Wyngaard JC, Coté OR (1972) The budgets of turbulent kinetic energy andd temperature variance in the atmospheric surface layer. *J Atmos Sci* 28: 190-201.

Wyngaard JC (1973) On surface-layer turbulence. In: Workshop on Micrometeorology (Ed. D.A. Haugen), *Am Met Soc* Boston, USA, 102-149.

Wyngaard JC, Clifford SF (1977) Taylor's hypothesis and the high-frequency turbulence spectra. *J Atmos Sci* 34: 922-929.

Wyngaard JC (1981) The effects of probe-induced flow distortion in atmospheric turbulence measurements. *J Appl Met* 20: 784-794.

Wyngaard JC (1982a) Boundary-layer modelling. In: Atmospheric Turbulence and Air Pollution Modelling, Eds. F.T.M. Nieuwstadt and H. van Dop. *Reidel Publ* Dordrecht, Holland. 69-106.

Wyngaard JC (1982b) Comments on "Flow distortion by supporting structures" by AC Dyer. *Bound Lay Met* 22: 263-265.

Wyngaard JC, BrostRA (1984) Top-down and bottom-up diffusion of a scalar in the convective boundary layer. *J Atmos Sci* 41: 102-112.

Wyngaard JC (1988) The effects of probe induced flow distortion on atmospheric turbulence measurements: Extension to scalars. *J Atmos Sci* 45: 3400-3412.

Zeman O, Jensen NO (1987) Modification of turbulence characteristica in flow over hills. *Quart J Roy Met Soc* 113: 55-80.

Zilitinkevich SS (1972) On the determination of the height of the Ekman boundary layer. *Bound Lay Met* 3: 141-145.

Zilitinkevich SS (1975) Resistance laws and prediction equations for the depth of the planetary boundary layer. *J Atmos Sci* 32: 741-752.

Zilitinkevich SS (1991) Turbulent penetrative convection. *Avebury Technical* Aldershot, UK, 179 pp.